UCLouvain

epl

École polytechnique de Louvain

Ant Colony Optimization for complex multi-objective supply chain problems

Application to the optimal deployment of green hydrogen in Belgium

Author: **Mathieu CHAMART**
Supervisor: **Francesco CONTINO**
Readers: **Davide TONELLI, Phillippe CHEVALIER**
Academic year 2021–2022
Master [120] in Mechanical Engineering

Abstract

By 2050, the demand of hydrogen for Europe and UK could reach up to 25% of the total final energy consumption. Most of the industrial demand is due to the production of chemicals, as ammonia or methanol, but also to refineries and steel industry. Today European hydrogen is mostly produced from fossil fuels by Steam Methane Reforming (SMR) while the current green alternatives cover less than 4% of the total hydrogen production. Through the integration of a hybrid metaheuristic algorithm, this work analyses the optimal hydrogen supply chain network design (HSCND) to decarbonize the industrial production of hydrogen in Belgium by 2050. While most literature focuses on optimizing the HSCND from financial perspectives, this study includes the environmental impact as second objective. The Pareto-optimality of cost and CO_2 emissions is studied based on the ϵ-constraint method. The hybrid metaheuristic is based on the integration of the Multi-Variate Ant Colony Optimization (ACO-MV) as master algorithm to handle the variables associated to the nonlinear constraints, while a classical Mixed Integer Linear Programming (MILP) solver is adopted for the solution of the slave problem. A parallel implementation, based on the simplification of the problem with the removal of the nonlinearities, was used to test the performance of the hybrid metaheuristic algorithm. The total demand in Belgium is estimated at 19.6 TWh/year, distributed between 7 plants where hydrogen can be produced from SMR and electrolysis or imported from abroad. The results of the case study show that the hybrid implementation offers similar performances compared to the simplified version. Both show a progressive replacement of the operating SMR plants by imported green hydrogen, neglecting electrolysis deployment which is less competitive. The financial impact for installing 1 GW of electrolysis plants in Belgium could cause up to 30% of cost increase compared to the optimal solution. A sensitivity analysis is finally conducted to observe the trend required from the market to make electrolysis in Belgium a profitable option. From worst to best scenario for the price of imported hydrogen, the price of European electricity should fall under 60€ or 80€/MWh respectively, compared to 100€/MWh considered in reference case.

Acknowledgement

I would first like to express gratitude to Davide Tonelli, for his support and advices on my master thesis during the year, but also to my supervisor, Professor Francesco Contino, who gave me the desire to choose this subject with his course about robust optimization of energy systems. I would also like to thank Phillipe Chevalier, who accepted to be part of my jury as reader.

Finally, I warmly thank my family and friends, for their encouragements and support, and especially my beloved Alexia for standing on my side.

Contents

List of Abbreviations

HSC Hydrogen Supply Chain
HSCDN Hydrogen Supply Chain Design Network
SMR Steam Methane Reforming
SMRs Steam Methane Reformers
DM Decision Maker
ACO Ant Colony Optimization
TSP Traveling Salesman Problem
AS Ant System
ACS Ant Colony System
SA Solution Archive
MOOP Multi-objective Optimization Problems
ASF Achievement Scalarizing Function
NSGAII Non Dominated Sorting Genetic Algorithm
PACO-MOFO Population based Ant Colony Optimisation for Multi-objective Function Optimization
MILP Mixed Integer Linear Programming
MINLP Mixed Integer Non-Linear Programming
CCS Carbon Capture and Storage
FEs Function Evaluations

Chapter 1

Introduction

By 2050, the European Union intends to become climate-neutral, with no net emissions of greenhouse gases [1]. This objective is at the center of the European Green Deal, which respects the engagements of the Paris Agreement, limiting the global temperature increase to well below 2°C and pursue efforts to keep it to 1.5°C [2]. The impact of global warming is transforming our environment, increasing the frequency and intensity of extreme weather events [3], and the trend will increase with the years, encouraging to strong and immediate actions.

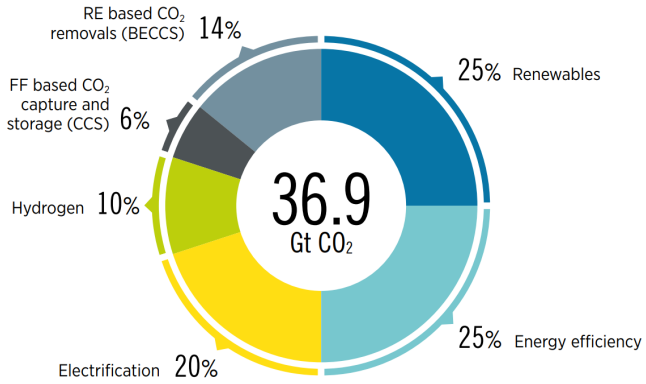

Figure 1.1: Reducing emissions by 2050 through six technological avenues [4]

Respecting the agreements of Paris would imply a cut of 37 gigatonnes of annual worldwide CO_2 emissions [4]. To achieve this objective, 6 technological avenues must be pursued actively, listed in Figure 1.1. The fifth key point concerns the production of clean hydrogen and its derivative fuels. Today, hydrogen is mainly used as a feedstock in industrial processes: refinery of crude oil, synthesis of chemicals as ammonia or methanol, or steel production. For the next 30 years, it is also expected to be a key player in energy applications, such as transport, heating or power sector. The demand in hydrogen will increase, and may reach 2,300 TWh per year for Europe and UK, corresponding to 20-25% of the total final energy consumption [5].

Yet, actual production of hydrogen is largely polluting. Despite its abundance on Earth, hydrogen does not exist naturally in its pure form in large quantities: it must be produced from other resources. Today, most of hydrogen is produced from hydrocarbons present in fossil fuels, notably through Steam Methane Reforming (SMR) of natural gas (grey hydrogen) or gasification of coal (black/brown hydrogen). However, alternatives methods exist to provide cleaner hydrogen, as electrolysis, producing hydrogen from water and electricity. If the electricity comes from renewable resources, the produced hydrogen has the denomination of green hydrogen. Green alternatives are representing a minority of hydrogen production: in Europe, about 300 electrolyzers are operating, covering less than 4% of the total hydrogen production [6].

The dual challenge is to increase the European decarbonized hydrogen production, while minimizing the impact of the infrastructure deployed. Most of literature focuses on financial impact, by optimizing the total cost of Hydrogen Supply Chain (HSC) and neglecting the environmental effect of a specific system design. Adding bi-objectivity on HSC optimization problems can produce a trade-off between cost and emissions, which are often antagonist. The set of optimal designs could be used to show to a Decision Maker (DM) the cost increase for different levels of decarbonization.

To answer this question, this master thesis focuses on the implementation of a metaheuristic algorithm in order to solve complex bi-objective hydrogen supply chain problems. Indeed, due to some non-linearities present in the modeling, metaheuristic could offer good performances compared to linear solvers. As initial approach, ACO, a promising metaheuristic technique, is adopted. The outcome of this work is a functional tool, applied to a case study of Belgium. The analyze focuses on the optimal deployment of green hydrogen in Belgium only, by investigating the progressive switch from existing Steam Methane Reformers (SMRs) to a green hydrogen production with time horizon 2050. The analysis intends to capture the trade-off between costs and CO_2 emissions through this transition.

This document has the following structure. First, a deep research is conducted about the best way to use ACO to solve multi-objective problems. It focuses on a literature review of the existing methods and the proposed approach, validated by tests on classical benchmark functions. Secondly, the mathematical HSC model used for the case study is described and explained in detail. It also includes explanations about the practical implementation of the multi-objective algorithm applied to the HSC model. The case study of Belgium is then analyzed in details. All the assumptions made and the input data are included, followed by the results on the reference case. The discussion of the results is followed by a conclusion and the perspectives.

Chapter 2

Multi-objective Ant Colony Optimization

2.1 Introduction to Ant Colony Optimization

Ant colony optimization (ACO) is a category of recent heuristic algorithms based on the natural behavior of an ant colony. It can be used in a large range of optimization problems, both for discrete and continuous search domains. In the discrete domain, one of the most famous applications of ACO is the Traveling Salesman Problem (TSP). Solving this problem means to find the shortest path connecting all the nodes of a graph and passing by each node once. Solving TSP with the "brute-force" method means that the algorithm must compute all possible roads, and then pick the shortest one. This approach would result in a complexity of $\Theta(n!)$. Other alternatives exist, such as Held–Karp algorithm, a dynamic programming algorithm having a complexity of $\Theta(2^n n^2)$ [7]. It is much lower than brute force, but still very consequent : for 100 nodes, the complexity would be of 10^{33} ! The use of non-exact method is then often required to solve this kind of problems.

The behavior of ants in nature is the following. When the ants want to find a source of food, they explore different paths to reach it. All the ants deposit on their path a chemical substance, called "pheromone", used to guide the future ants. If two paths are connecting the nest and the source of food, if the first is shorter than the second, more ants will be able to follow it, based on a larger amount of pheromone dropped on it. This process is described in Figure 2.1.

The first version of ACO, called Ant System (AS) was introduced by Marco Dorigo in 1991 [8], and was then developped and upgraded using many different techniques, to make it more effective and robust [9],[10],[11].

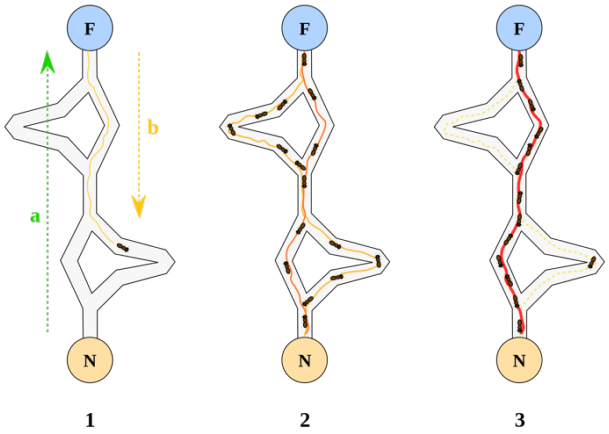

Figure 2.1: Example of behavior of ant colony: at stage 3 all the ants go trough the same path[12]

The first version of the algorithm uses a certain number of agents, called the "ants", making their own path through the graph following the state transition rule. The probability for an ant to go from node r to s, noted $p_k(r,s)$, depends on the desirability of the segment between r and s. The desirability is represented by 2 elements: the quantity of pheromone dropped on this segment, $\tau(r,s)$, and the inverse of the distance between the 2 nodes, $\eta(r,s)$, favoring shorter paths.

$$p_k(r,s) = p_k(r,s) = \begin{cases} \frac{[\tau(r,s)]\cdot[\eta(r,s)]^\beta}{\sum_{u\in J_k(r)}[\tau(r,u)]\cdot[\eta(r,u)]^\beta}, & \text{if } s \in J_k(r) \\ 0, & \text{otherwise} \end{cases} \tag{2.1}$$

In the equation, $J_k(r)$ is the set of nodes that has still to be visited by ant k on node r, and β is a parameter which determines the relative importance of pheromone versus distance. In this way, the shortest segments and consequently the segments that are the most visited are preferably chosen.

When all the m ants have achieved their travel, corresponding to the end of each iteration, there is only one global updating of the pheromone. Depending on the quality of their travel, each ant drops a certain quantity of pheromone on the segments taken, $\sum_{k=1}^{m}\Delta\tau_k(r,s)$. The lowest is the length of their tour L_k, the highest is the quantity of pheromone $\tau_k(r,s)$. Finally, a fraction α of the pheromone is removed, in a step called "evaporation", in order to reduce the role of the deposition of pheromone in the initial iterations.

$$\tau(r,s) \leftarrow (1-\alpha)\cdot\tau(r,s) + \sum_{k=1}^{m}\Delta\tau_k(r,s) \tag{2.2}$$

$$\Delta\tau_k(r,s) = \begin{cases} \frac{1}{L_k}, & \text{if } (r,s) \in \text{ tour done by ant } k \\ 0, & \text{otherwise} \end{cases} \tag{2.3}$$

We state that the algorithm converges when the difference between the solution in time t and t+1 will be less than a certain quantity ϵ. This difference can be either absolute or relative, depending on the user preference.

The major limitation of this version is the lack of enhancement for the best solutions. With the state transition rule, if a new optimal solution appears, the updating of pheromone can be not strong enough to enhance this particular solution, compared to the other segments. In order to improve AS, 3 major implementations were considered :

- Ant Colony System (ACS) [13]: it uses an adapted state transition rule to better tune exploitation versus exploration, but also a mechanism combining global and local updating of the pheromone. ACS allows to be more sensitive to the best paths and have a better exploitation of the best solutions.
- Min-Max: this implementation aims to enhance the best solutions, as ACS, but also the risk of stagnation of the search. To deal with the stagnation issue, a lower and upper bounds are imposed to the pheromone deposition, limiting the possibility of too early convergence. These bounds can evolve dynamically, and the convergence is achieved when lower and upper bounds of pheromone deposited are stabilized.
- Elitist: it introduces a new type of agents: elitist ants, that have a memory larger than classical ants, and are able to know the best solution found by the entire colony.

The complete description of these other formulations of AS can be found in Appendix A.

2.2 Continuous single objective ACO

The previous section decribed a few implementations of ACO, designed to deal with discrete variable problems, like the Traveling Salesman Problem. However, in practical cases, the search space is rarely discrete. For solving the hydrogen supply chain problem and finding an optimal design, it would be necessary to find an alternative to make ACO suitable for continuous search domains.

2.2.1 $\mathbf{ACO_R}$

The most known implementation, developed by Socha and Dorigo in [14], is called ACO_R. In the previous sections, the pheromone model was built as a finite set of discrete components, like a matrix of pheromone. To deal with continuous variables, another type of pheromone model is required. ACO_R uses a Solution Archive (SA), giving a probabilistic distribution to guide the search. The solution archive contains a given set of complete solutions of the problem. While a pheromone model in combinatorial optimization can be seen as an implicit memory of the search history, a solution archive is an explicit memory

[15].

The algorithm starts by initializing the SA with k randomly chosen solutions. Each solution is described by a finite set of variables $[x_1, x_2, ...x_n]$, with corresponding objective function $f(x_1, x_2, ...x_n)$. The solutions are then sorted: the ranking of a solution depends on the value of the objective function applied to the solution. Each solution s_j is also associated to a given weight ω_j, linked to its rank, $rank(s_j)$:

$$\omega_j = \frac{1}{qk\sqrt{2\pi}} e^{\frac{-(rank(s_j)-1)^2}{2q^2k^2}}, \tag{2.4}$$

where q is a parameter of the algorithm. The next step is the construction of m new solutions, m being in classical AS the number of ants. For each ant, it chooses probabilistically a given solution in the set of k solutions of SA, s_{search}. This solution is chosen as a base for exploration and construction of a new solution. The probability to choose a solution j as a base for exploration, p_j, depends on its weight, and is given by:

$$p_j = \frac{\omega_j}{\sum_{l=1}^{d} \omega_l} \tag{2.5}$$

Once a solution is selected as s_{search} in SA, exploration around the solution can occur. The ant samples the neighborhood by building a gaussian probabilistic density function (PDF) around the solution, given by:

$$g(x, \mu_{search}, \sigma_{search}) = \frac{1}{\sigma_{search}\sqrt{2\pi}} e^{-\frac{(x-\mu_{search})^2}{2\sigma^2_{search}}}, \tag{2.6}$$

where the mean μ_{search} is the solution s_{search}, and the standard deviation σ_{search} is expressed as:

$$\sigma_{\text{search}} = \xi \sum_{r=1}^{k} \frac{|s_r - s_{\text{search}}|}{k-1} \tag{2.7}$$

Then, a new solution is chosen probabilistically in the neighborhood according to the built Gaussian PDF. Note that the ζ parameter is similar to the ρ parameter in the decay process in classical ACO: it influences the speed of convergence. The representation of the solution archive and the sampling around a solution s_{search} is represented in Figure 2.2.

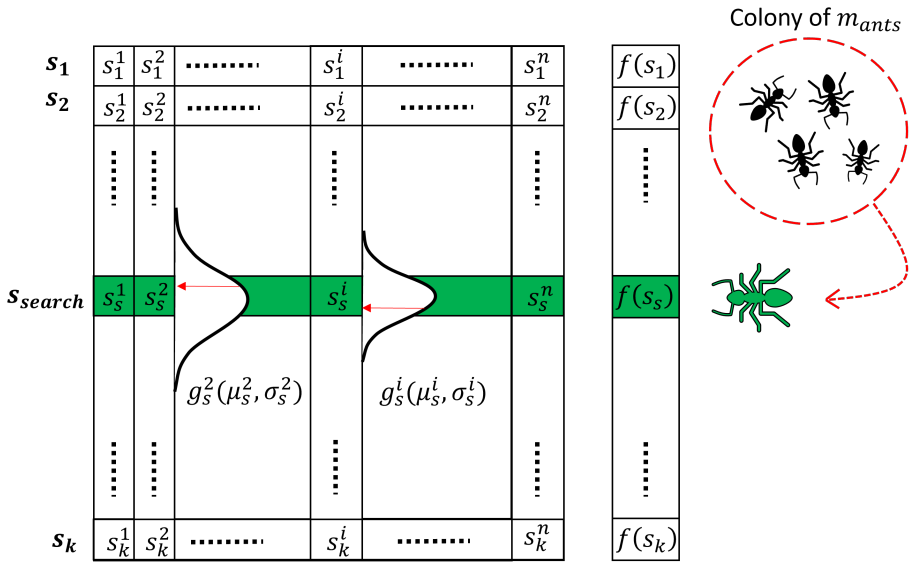

Figure 2.2: Solution archive representation

Once all the new solutions are created, the $k + m$ solutions are ranked and again sorted, and only k top solutions are kept in SA for the next iteration. The whole process is repeated at each iteration, until the criteria of convergence fixed is satisfied. Practically, a maximum number of function evaluations can also be imposed, limiting the computational time or removing the possibility to run indefinitely due to non-convergence. The process is summarized in Figure 2.3.

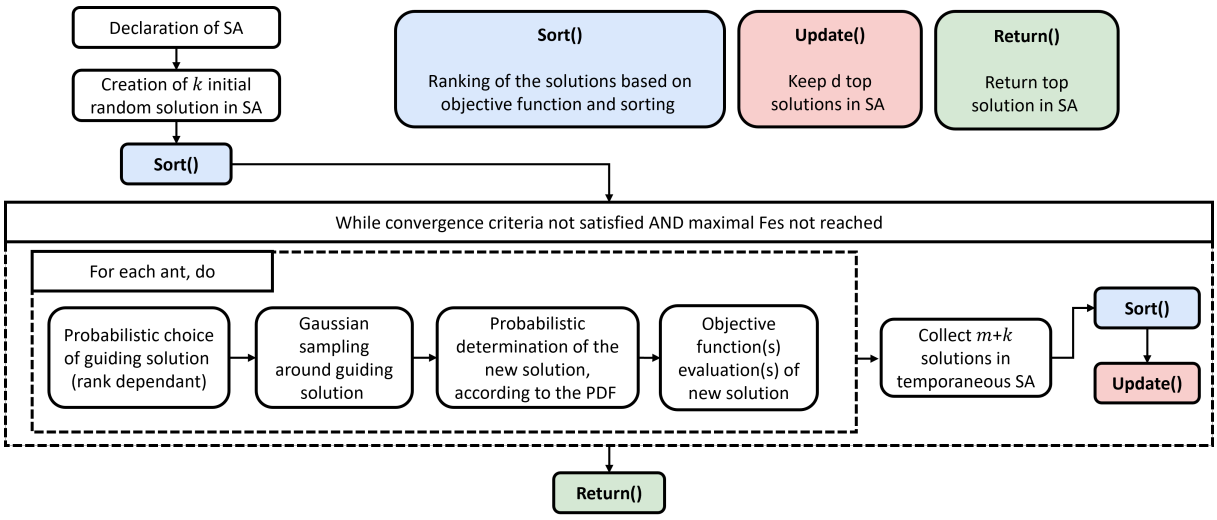

Figure 2.3: Flow chart of ACO_R

2.2.2 ACO_{MV}

Many real life optimization problems can be modeled using not only continuous variables, but a combination of continuous and discrete variables. Socha and Dorigo developed an extension of the classical ACO_R to also tackle discrete variables [15]. Their algorithm is called ACO_{MV}, where MV stands for multivariate. It allows the user to explicitly declare each variable as continuous, ordinal, or categorical. Ordinal means that there is an ordering, for example integers, and categorical that the value depends of a finite set of categories that is unordered. Continuous variables are handled with a continuous optimization approach (ACO_R), ordinal variables are handled with a continuous relaxation approach ($ACO_{MV\text{-}o}$), and categorical variables are handled with a categorical optimization approach ($ACO_{MV\text{-}c}$)[15].

The main steps of ACO_R remain similar, except that the variables are stored separately in solution archive (see in Figure 2.4) and that the probabilistic construction of solution is different depending of the type of variable. There is then successively a solution construction for ACO_R, $ACO_{MV\text{-}o}$ and $ACO_{MV\text{-}c}$.

For ordinal variables, $ACO_{MV\text{-}o}$ does not operate on their actual values but on their indices in the solution archive. The values of the indices for the new solutions are generated as real numbers, as in ACO_R. The only difference is that, before the evaluation of the objective function, the continuous values are rounded to the nearest valid index. The value at that index is then used for the objective function evaluation. This process is called relaxation of the variables. Categorical variables have also their own construction method, which is not presented since it is not in the scope of this work.

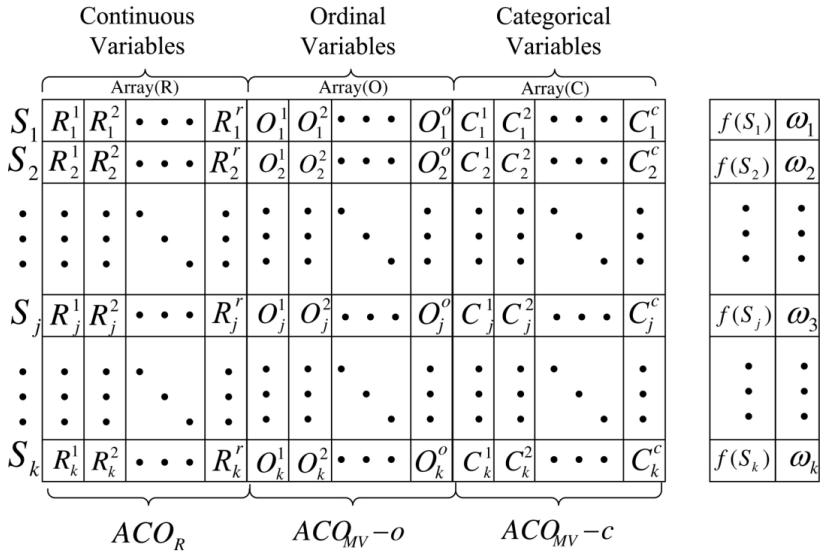

Figure 2.4: Solution archive in ACO_{MV} [15]

2.3 Multi-objective optimization

2.3.1 Concepts

Many situations require the engineers to deal with Multi-objective Optimization Problems (MOOP): it means that several different objectives have to be simultaneously minimized (or maximized). Rigorously, solving a problem of optimization of K objectives (here minimization problem) resumes to find:

$$\begin{gathered}\text{Min } f(x) = (f_1(x), f_2(x), ..., f_K(x)),\\ \text{with } x = (x_1, x_2, \ldots, x_n) \in X\end{gathered}$$

To define a classification to establish the best solutions, the concept of dominance is introduced. A decision vector $a \in X$ dominates another $b \in X$ ($a \succ b$) if, and only if

$$\begin{gathered}\forall i \in \{1, 2, \ldots, K\} \mid f_i(a) \leqslant f_i(b) \wedge\\ \exists j \in \{1, 2, \ldots, K\} \mid f_j(a) < f_j(b)\end{gathered}$$

The set of all non-dominated solutions is called "Pareto-front", in which all the solutions are equivalently optimal, representing the trade-off between the objectives.

2.3.2 Classical methods for solving MOOP

To solve multi-objective problems, many classical optimization methods exist. The output of the optimization process is often submitted to a decision maker (DM) who needs a solution. These techniques can be divided in 4 categories, illustrated in Table 2.1.

Methods	Description	Examples
No-preference	Returns some neutral compromise solution	Method of global criterion
A priori	DM expresses preferences about the different objectives, and the closest solution is found.	Value function method, lexicographic ordering, goal programming, ...
A posteriori	Generates the whole set of Pareto optimal solutions. Then DM selects one solution among the set.	Weighting method, ϵ-constraint method, method of weig. metrics, ASF approach ...
Interactive	Based on an iterative search process, a solution pattern is formed and repeated iteratively	GDF method, GUESS method, Tchebycheff method, NIMBUS method, ...

Table 2.1: Classical methods for solving MOOP [16]

A priori methods have as advantage to have a very low computational cost. However, the major limitation is that, without knowing the problem in detail, it can be very hard to express preferences among the different objectives. It can be problematic for the decision maker if he is not aware of all the specificities of the problem.

An example of a priori methods is the lexicographic ordering. The decision maker must specify an absolute order for the different objectives. If the most important objective has a unique optimal value, then the process stops. If not, the second most important objective is optimized, ensuring that the first one is still optimal, and so on until the optimum is found. Then, the order of importance of objectives can affect drastically the solution, as objectives of lower importance may have no impact on the final solution. Moreover, any idea of trade-off is impossible, since it returns a single solution.

In interactive methods, a solution pattern is formed and repeated iteratively. These methods require a true implication for the decision maker, who must invest time and cooperation to direct the solutions process.

Finally, the last class concerns a posteriori methods, which return not only a single point, but the whole Pareto front. From this, the decision maker can choose, with higher-level information, a solution among the Pareto set. [17]. The process is summarized in Figure 2.5. Contrary to interactive methods, the decision maker is not involved in the optimization before the end of the process. The main drawback of these methods is that the computational cost is higher.

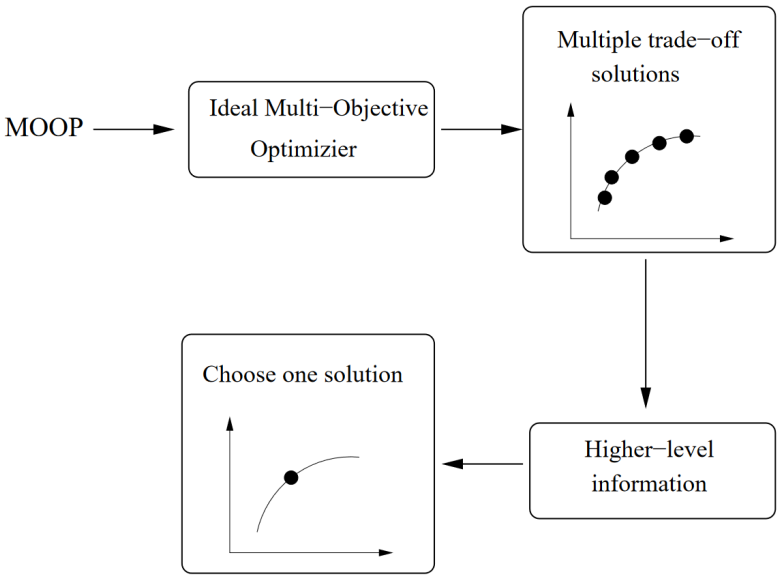

Figure 2.5: A posteriori methods procedure [17]

A posteriori methods are the best suited for our application, since the objective is to capture a trade-off in the set of solutions without involving the decision maker. The price

to pay is the computational cost. The simplest a posteriori method is called weighting method. The idea is to map all objective functions into a single objective function, which is the weightened sum of all other objective functions, that is then optimized.

$$\begin{array}{ll} \text{minimize} & \sum_{i=1}^{k} w_i f_i(\mathrm{x}) \\ \text{subject to} & \mathrm{x} \in S, \\ \text{where} & \sum_{i=1}^{k} w_i = 1 \\ & w_i \geq 0 \ \forall i = 1, \ldots, k. \end{array} \tag{2.8}$$

However, despite being very simple, it has many drawbacks. One of the most important is that even if the weights are evenly distributed, it does not necessarily produce evenly distributed representation of the Pareto set. Moreover, slight changes in weightings values can impact drastically the solution, bringing undesired versatility.

Another very popular method in multi-objective optimization methods is the ϵ-constraint method. We can summarize it like that: the idea is to optimize only one objective function, while keeping the others constrained under a level ϵ. Then, by varying the value of ϵ between fixed limit values, we can retrieve a complete set of Pareto-optimal solutions. It is a quite robust method, even if the setting of lower and upper bounds for ϵ can be a non-trivial task.

$$\begin{array}{ll} \text{Minimize} & f_l(x) \\ \text{Subject to} & f_j(x) \leq \epsilon_j, \text{ for all } j = 1, \ldots, k, j \neq l \\ & x \in S \end{array} \tag{2.9}$$

Finally, the Achievement Scalarizing Function (ASF) is also a well-known technique in the field, which is also a mapping of all objective functions into a single one.

$$\begin{array}{ll} \text{Minimize} & \mathrm{S}_g(f(x)) = \max_{\mathrm{i}=1,\ldots,\mathrm{k}} \left[w_{\mathrm{i}} \left(f_{\mathrm{i}}(\mathbf{x}) - g_{\mathrm{i}} \right) \right] \\ \text{subject to} & \mathrm{x} \in S, \\ \text{where} & \sum_{i=1}^{k} w_i = 1 \\ & w_i \geq 0 \ \forall i = 1, \ldots, k \end{array} \tag{2.10}$$

where w_i are fixed scaling factors and $\boldsymbol{g} \in \mathfrak{R}^{\mathrm{k}}$ is the reference point specified by the DM, with its components representing the desired values of the objective functions. However, it is mainly used when the number of objectives exceeds 3.

Most of the time, these techniques are used with classical exact solver. However, in practice the choice of the optimizer is free, and some metaheuristic algorithms, like genetic algorithms, can also be easily hybridized with these techniques.

2.3.3 Multi-objective ACO

Apart from classical methods, a large range of metaheuristic algorithms were developped through the years to deal with multi-objective problems. As this master thesis focuses on

Ant Colony, a complete overview of the existing techniques using ACO is realised in the next sections.

As the first purpose of ACO was to solve discrete problems, like the Traveling Salesman problem, most of the existing formulations developed to deal with multi-objective are suited for discrete domains. To sort all the proposed versions, a taxonomy was proposed in [18] and in [19], classifying the methods by 5 criterias:

- form of pheromone matrix (multiple, single),
- solution construction (target, dynamic, fixed),
- evaluation (Pareto, non-Pareto),
- update and decay (global, individual),
- pareto archival (online, offline, elite, none),

However, these techniques are especially designed for solving TSP. Other techniques were developed, able to tackle continuous search domains.

$\mathbf{MOACO_R}$

The first method using ACO_R to solve multi-objective problems was developed by researchers from University of Birmingham [20]. The developped method, $MOACO_R$, differs from classical ACO_R only for the method used to collect and store the solutions in the archive. Contrary to single objective optimization, the best solutions in the ranking do not maximize only one objective function, but are trying to be closer to the theoretical Pareto front, representing the trade-off between the different objectives. Some other methods are then needed to rank the solutions and select which solutions will be used as search base for the exploration phase. To rank the set of solutions, the concept of dominance depth is used: the solutions are ranked in multiple fronts, where in each front no solution dominates another. For example, the rank of 1 is attributed to the best front, so the outer front, the closest to the theoretical Pareto front. This concept is illustrated in Figure 2.6.

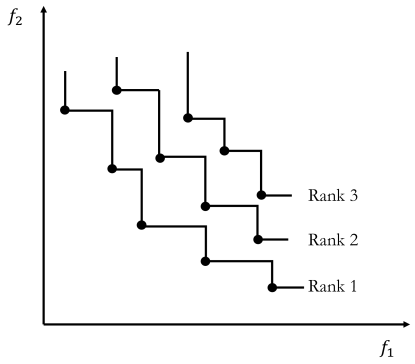

Figure 2.6: Dominance depth concept. Solutions are sorted into fronts of relative importance. Within a front all the solutions are equivalent.

The procedure of fast non dominated sorting is taken from the Non Dominated Sorting Genetic Algorithm (NSGAII) algorithm [21], and is presented in Figure 2.7 First, it computes two entities for each solution p in the set of solutions: the domination count n_p, being the number of solutions dominating the solution p, and S_p, being the set of solutions that the solution p dominates itself. The procedure is the following: it begins with the first non-dominating front, so all the solutions with $n_p = 0$. Then, for each solution in the first front, it goes through its set S_p: all the n_p of the set are lowered by 1. The solutions in S_p having $n_p = 0$ are part of the second non-dominated front, and are placed in a new set Q of solutions. In the next step, the algorithm will go through the set Q, and repeat the procedure, identifying the 3rd front, and so on, until all the fronts are ranked.

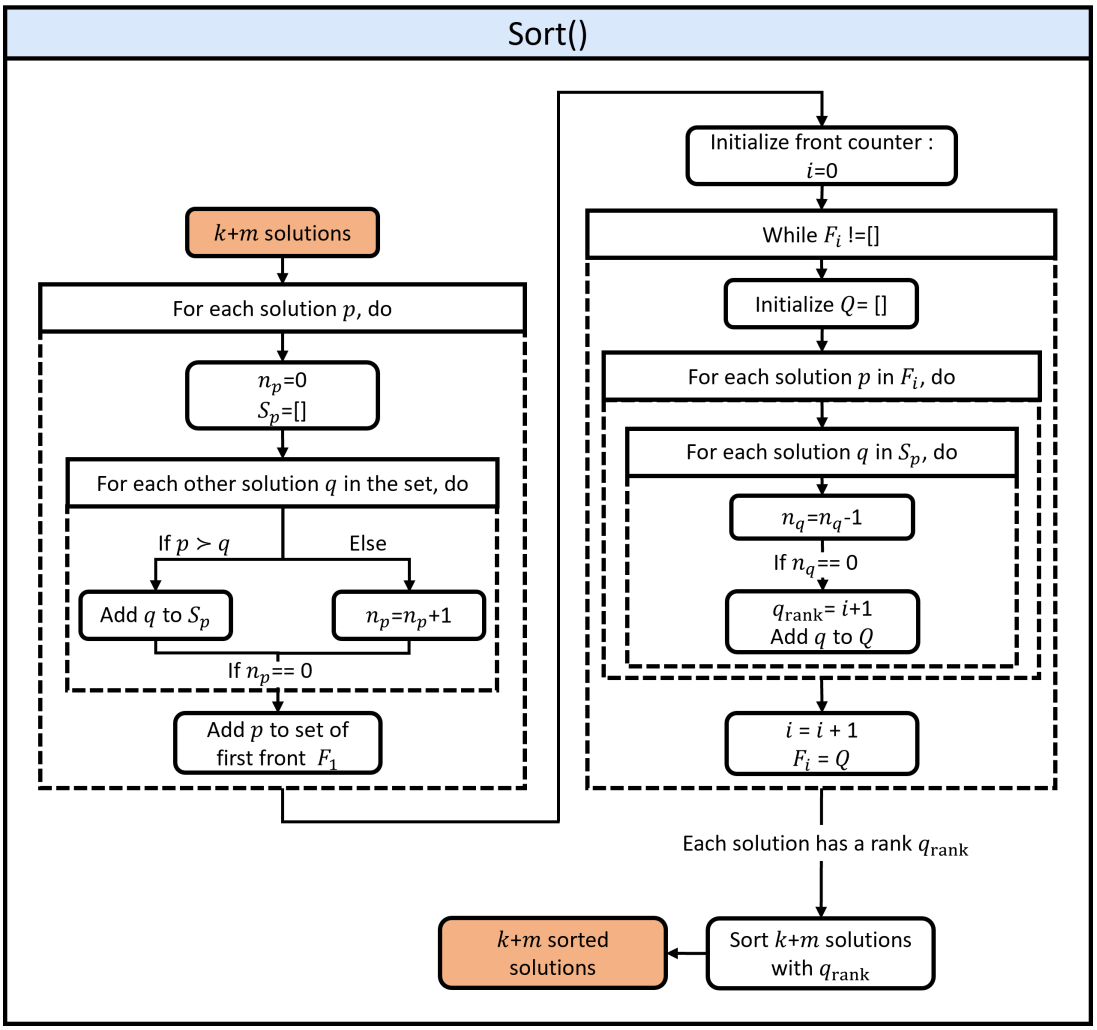

Figure 2.7: Fast Non Dominated Sorting in MOACO_R

If the number of solutions still exceeds the size of the archive, then another selection process engages, based on the crowding distance. Generalized to n-dimensions, it can be measured by the average side length of the cuboid in the objective space. A graphical

representation is shown in Figure 2.9. The lower is the crowding distance, the lower is the chance for the solution to be kept in the archive: this system favorizes the diversity through the Pareto front. The complete updating procedure is described in Figure 2.8. Except these specific aspects, the ACO_R process stays unchanged. Sorting and updating processes, shown in Figure 2.7 and Figure 2.8, can be directly integrated in flowchart of ACO_R presented in Figure 2.3.

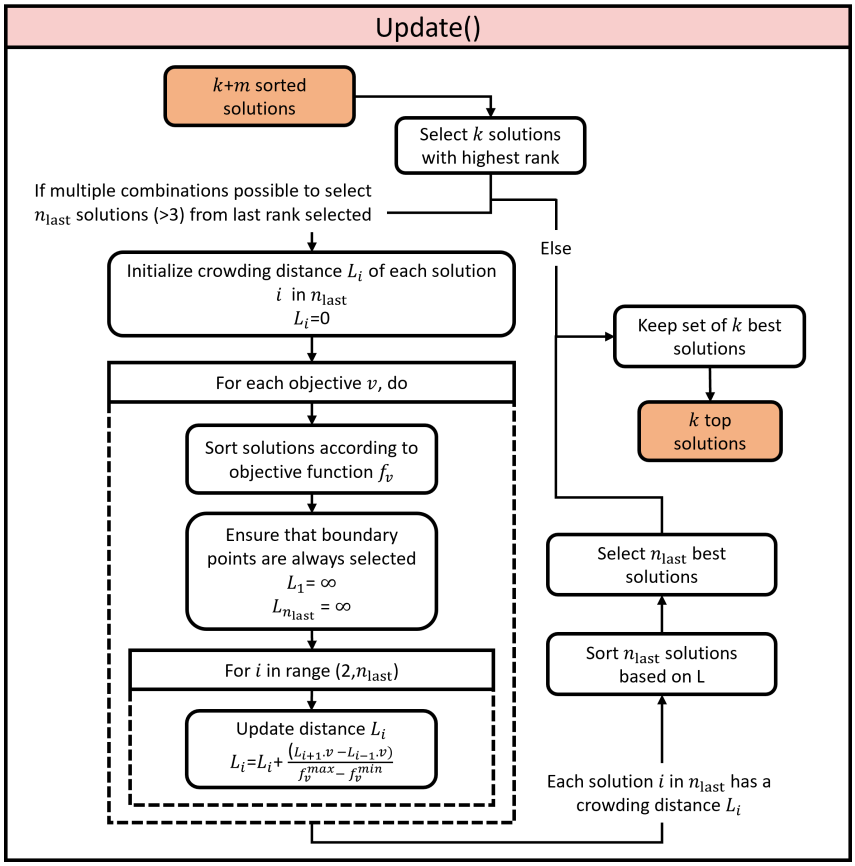

Figure 2.8: Updating process in $MOACO_R$

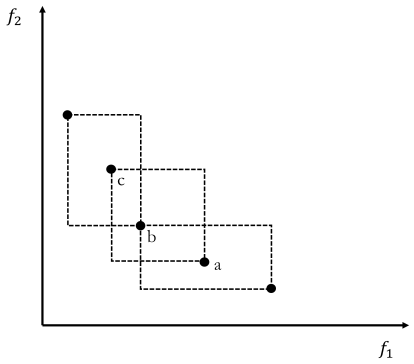

Figure 2.9: Crowding distance concept. Here, crowding distance c is larger than a than b.

PACO-MOFO

The idea proposed by Daniel Angus [22] is the same than the previous versions: modify the ranking model of classical ACO_R. In their version, Population based Ant Colony Optimisation for Multi-objective Function Optimization (PACO-MOFO), the ranking is done according to NSGAII. It is followed by a fitness procedure, setting the fitness of each population as inverse of rank. Then, the process of fitness sharing starts: it derates the fitness of a solution x by an amount that represents its similarity to other individuals in the population [23]. The sharing function $\mathrm{sh}(x, y) \in [0, 1]$ expresses this similarity between solution x and y: if there is no similarity, then it is 0. The objective is that, if two solutions are similar, they share the same fitness. Note that several expressions for the sharing function exist, depending on the topology of the problem. Here is an example of sharing function [23], and the expression of the shared fitness for a population P:

$$\begin{aligned} f(x, P) &= \frac{f(x)}{\sum_{y \in P} \mathrm{sh}(x, y)} \text{ and } f(P) = \sum_{x \in P} f(x, P) \\ \mathrm{sh}(x, y) &= \max\left\{0, 1 - (d(x, y)/\sigma)^{\alpha}\right\} \end{aligned} \tag{2.11}$$

Finally, it comes to select the solutions in archive that will be used to generate new solutions, a probabilistic rule is applied, based on the fitness raised to a history exponent power fitness α.

Then, the second important change concerns the replacement of the solutions, here done using a specific crowding technique: the Restricted Tournament Selection (RTS). RTS selects a random subset of the population of the crowding window size, and compares the new solution found against the closest match of the solution in the subset. The best solution, here the one strongly dominating, is kept while the other is discarded [22]. An important parameter is the size of the crowding window, which can be adapted to the topology of the problem.

iMOACO$_R$

iMOACOR [24] is an extended version of ACO_R which is able to deal with problems with more than 3 objectives, like NSGAIII outperforming NSGAII. The authors proposed an indicator-based ranking algorithm to establish different quality levels among solutions produced by ant: the R2 indicator. However, as iMOACO$_R$ is especially designed to deal with many-objectives problems, it is not relevant to develop it further in this document, since the research is focused on bi-objective problems.

The summary of the research conducted about ACO is shown in Figure 2.10, with methods covering discrete or continuous search domains and able to handle single or multi objective problems.

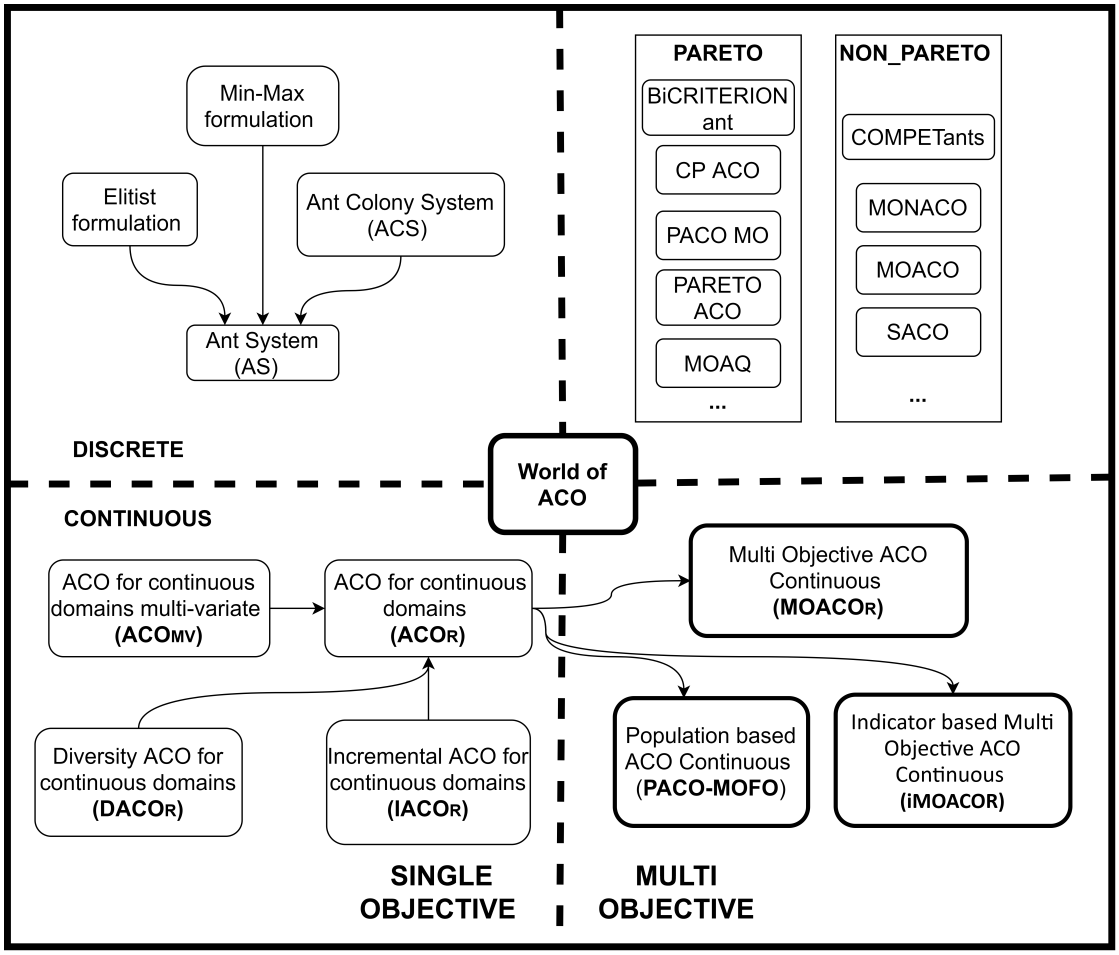

Figure 2.10: Overview of existing ACO methods, dealing with discrete/continuous single/multi objective problems

2.3.4 Comparison

In order to solve HSCD optimisation problem with ACO, a method must be chosen. Based on the previous researches, two options appear:

- Choose a classical a posteriori method for solving MOOP and hybridize this method with ACO
- Choose an existing method based on ACO, like MOACO_R or PACO-MOFO

Both MOACO_R and PACO-MOFO are relevant for solving multi-objective problems. The problem is that they are really similar to NSGAII [21]: the only difference is the search model. ACO is comparable to genetic algorithms on the level of performances, yet it does not offer better results. Then, MOACO_R has no added value compared to NSGAII, which is a state of the art method in metaheuristic multi-objective optimization. Moreover, the presence of MOACO_R in the literature is very sparse, and it seems that this technique is not very used and developed.

On the other hand, a hybrid version of a classical method could offer many advantages. Despite a higher computational cost, these methods are robust, but also allow to use the single objective optimizer as a "black box". In our case, it can be ACO_R, but also an exact solver that could be used to test the metaheuristic implementation. It is quite different for $MOACO_R$ for example, that needs a modification of the ranking process of ACO_R, and that would not allow a comparison with exact solvers.

In the different a posteriori techniques described in subsection 2.3.2, not all are suited for our problem. ASF, for example, is especially designed for multi-objective problems with more than 3 objective functions, and is not relevant to be used in this study, as only 2 objectives would be considered. In general, we can state that ϵ-constraint method is more popular for bi-objective problems than for multi-objective problems with higher dimension. Contrary to the weighting method, where a slight change in the weights can affect drastically the solution, a change of the level of increment for the ϵ-constraint does not affect the set of solutions, but only the density of the Pareto set. Moreover, it can be easily combined with metaheuristics. For example, in [25], an hybridization of evolutionary algorithm with ϵ-constraint is realized. The authors prove that this version is very competitive in comparison with NSGAII, mainly regarding the quality of solutions (spread, convergence, ...).

As a conclusion, the method chosen to tackle our research problem is then an ϵ-constraint method hybridized with ACO_R, that will be called as ϵ-ACO_R. The hybridization and the tests conducted for the validation are described in the next section.

2.3.5 Proposed version

Implementation

The implementation of ϵ-ACO_R realized for this work is inspired from the approach described in [25], with the hybridization of an evolutionary algorithm with the ϵ-constraint method. In this case, it is adapted to use ACO_R as single objective optimizer. The actual implementation is described in Algorithm 1. Initially, the Pareto set P is empty. In a first step, the upper and lower bounds (ub, lb) must be computed. It is done by optimizing separately the first and second objective functions, and then by evaluating the second objective function for these two solutions. Note that it could also be done in the other way around, by evaluating the first objective function. Once the upper and lower bounds are computed, the level of ϵ is progressively increased by a given increment, depending on the parameter p, which is the desired density of the Pareto set. While ϵ is lower than the upper bound, the first objective function is optimized, while keeping the second objective function constrained under ϵ. After each single-objective optimization process, the found solution is compared to the actual Pareto set. If it is non-dominated, then it is added to the set, removing eventual dominated solutions. This novel approach would bind the supposed robustness of ϵ-constraint and the metaheuristic advantages from ACO_R.

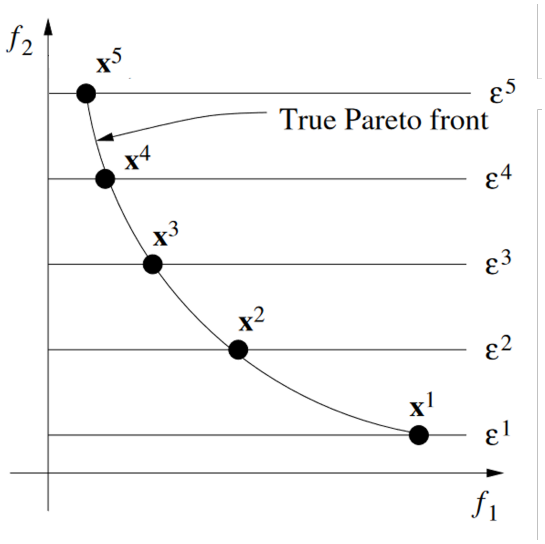

Figure 2.11: Generating different solutions with the ϵ-constraint method [25]

Algorithm 1 ϵ-ACO$_\mathrm{R}$

Input: Desired Pareto density p
Output: Pareto set P

$P \leftarrow \emptyset$
$ub \leftarrow f_2(\mathrm{ACO_R}(f_1))$
$lb \leftarrow f_2(\mathrm{ACO_R}(f_2))$
$\epsilon \leftarrow lb$
$d\epsilon \leftarrow \dfrac{ub - lb}{p}$
while $\epsilon \leq ub$ **do**
  $x \leftarrow \mathrm{ACO_R}(f_1, \epsilon)$
  if x non dominated with respect to P, **then**
    $P \leftarrow P - \{y \in P | x \succ y\}$
    $P \leftarrow P \cup \{x\}$
  end if
  $\epsilon \leftarrow \epsilon + d\epsilon$
end while

Tests and validation

A series of tests is conducted on classical benchmark functions for bi-objective problems. The complete list of tested objective functions is given in Table 2.2. The objective is to demonstrate that ϵ-ACO$_\mathrm{R}$ can offer good performances compared to classical metaheuristic techniques. For these tests, it is compared to NSGAII, and the comparizon is made on multiple criterias, as the density and the spread of set of solutions, Pareto optimality, ...

Name	Objective functions	Search domain	Comments
SCH1	$f_1(x) = x^2$ $f_2(x) = (x-2)^2$	$-100 \leq x \leq 100$	Convex
KUR	$\begin{cases} f_1(\boldsymbol{x}) = \sum_{i=1}^{2} \left[-10 \exp\left(-0.2\sqrt{x_i^2 + x_{i+1}^2}\right)\right] \\ f_2(\boldsymbol{x}) = \sum_{i=1}^{3} \left[\lvert x_i\rvert^{0.8} + 5\sin\left(x_i^3\right)\right] \end{cases}$	$-5 \leq x_i \leq 5$ $1 \leq i \leq 3$	Nonconvex
FON	$\begin{cases} f_1(\boldsymbol{x}) = 1 - \exp\left[-\sum_{i=1}^{n}\left(x_i - \frac{1}{\sqrt{n}}\right)^2\right] \\ f_2(\boldsymbol{x}) = 1 - \exp\left[-\sum_{i=1}^{n}\left(x_i + \frac{1}{\sqrt{n}}\right)^2\right] \end{cases}$	$-4 \leq x_i \leq 4$ $1 \leq i \leq 30$	Nonconvex
ZDT1	$\begin{cases} f_1(\boldsymbol{x}) = x_1 \\ f_2(\boldsymbol{x}) = g(\boldsymbol{x}) h\left(f_1(\boldsymbol{x}), g(\boldsymbol{x})\right) \\ g(\boldsymbol{x}) = 1 + \frac{9}{29}\sum_{i=2}^{30} x_i \\ h\left(f_1(\boldsymbol{x}), g(\boldsymbol{x})\right) = 1 - \sqrt{\frac{f_1(\boldsymbol{x})}{g(\boldsymbol{x})}} \end{cases}$	$0 \leq x_i \leq 1$ $1 \leq i \leq 3$	Convex
ZDT2	$\begin{cases} f_1(\boldsymbol{x}) = x_1 \\ f_2(\boldsymbol{x}) = g(\boldsymbol{x}) h\left(f_1(\boldsymbol{x}), g(\boldsymbol{x})\right) \\ g(\boldsymbol{x}) = 1 + \frac{9}{29}\sum_{i=2}^{30} x_i \\ h\left(f_1(\boldsymbol{x}), g(\boldsymbol{x})\right) = 1 - \left(\frac{f_1(\boldsymbol{x})}{g(\boldsymbol{x})}\right)^2 \end{cases}$	$0 \leq x_i \leq 1$ $1 \leq i \leq 30$	Nonconvex
ZDT4	$\begin{cases} f_1(\boldsymbol{x}) = x_1 \\ f_2(\boldsymbol{x}) = g(\boldsymbol{x}) h\left(f_1(\boldsymbol{x}), g(\boldsymbol{x})\right) \\ g(\boldsymbol{x}) = 91 + \sum_{i=2}^{10}\left(x_i^2 - 10\cos\left(4\pi x_i\right)\right) \\ h\left(f_1(\boldsymbol{x}), g(\boldsymbol{x})\right) = 1 - \sqrt{\frac{f_1(\boldsymbol{x})}{g(\boldsymbol{x})}} \end{cases}$	$0 \leq x_1 \leq 1$ $-10 \leq x_i \leq 10$ $2 \leq i \leq 10$	NonConvex
ZDT6	$\begin{cases} f_1(\boldsymbol{x}) = 1 - \exp\left(-4x_1\right)\sin^6\left(6\pi x_1\right) \\ f_2(\boldsymbol{x}) = g(\boldsymbol{x}) h\left(f_1(\boldsymbol{x}), g(\boldsymbol{x})\right) \\ g(\boldsymbol{x}) = 1 + 9\left[\frac{\sum_{i=2}^{10} x_i}{9}\right]^{0.25} \\ h\left(f_1(\boldsymbol{x}), g(\boldsymbol{x})\right) = 1 - \left(\frac{f_1(\boldsymbol{x})}{g(\boldsymbol{x})}\right)^2 \end{cases}$	$0 \leq x_i \leq 1$ $1 \leq i \leq 10$	Nonconvex, nonuniformly spaced

Table 2.2: Benchmark objective functions

The ϵ-ACO$_R$ algorithm was implemented in Python, respecting the flowcharts given in 1 and Figure 2.3. The NSGAII version used for the comparison comes from [26], an open source multi-objective optimization module in Python. The graphical results for each test function are represented in the figures below, with the Pareto front comparison between NSGAII and ϵ-ACO$_R$.

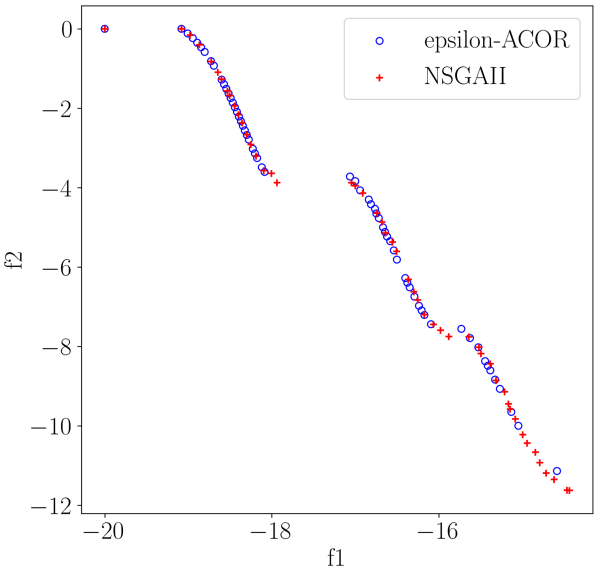

Figure 2.12: Kursawe function

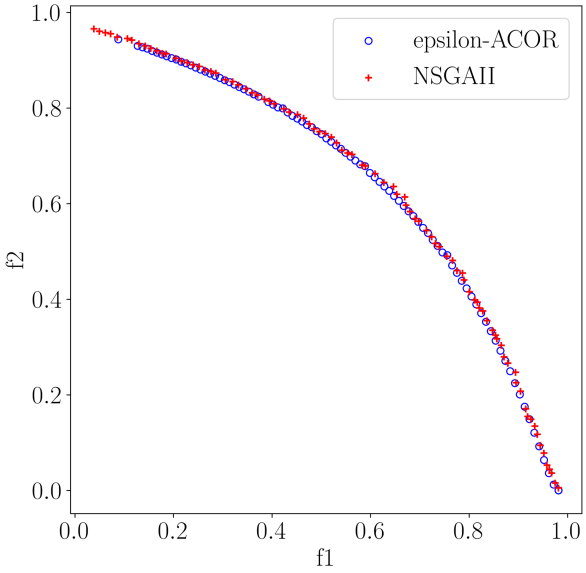

Figure 2.13: Fonseca function

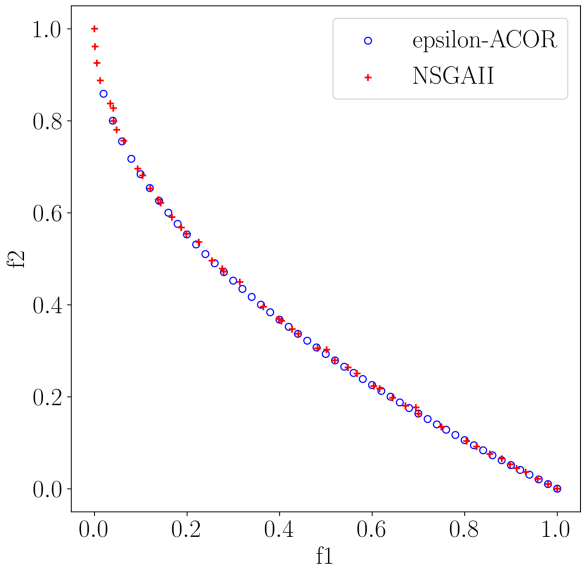

Figure 2.14: ZDT function 1

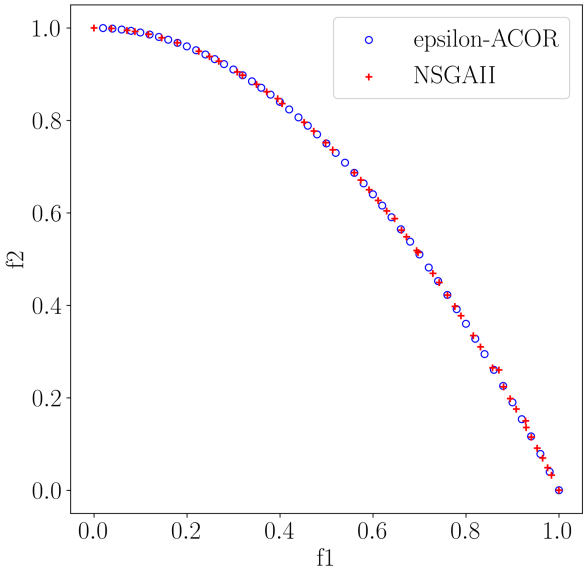

Figure 2.15: ZDT function 2

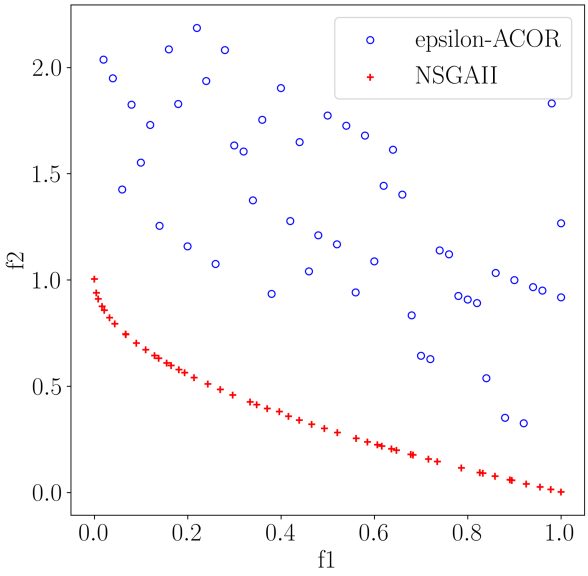

Figure 2.16: ZDT function 4

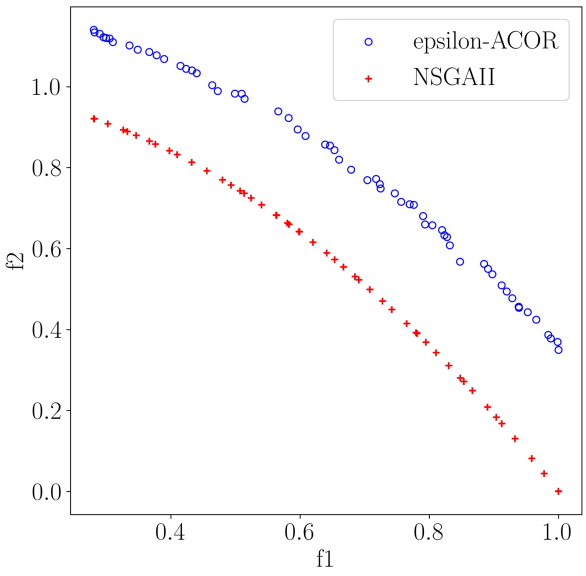

Figure 2.17: ZDT function 6

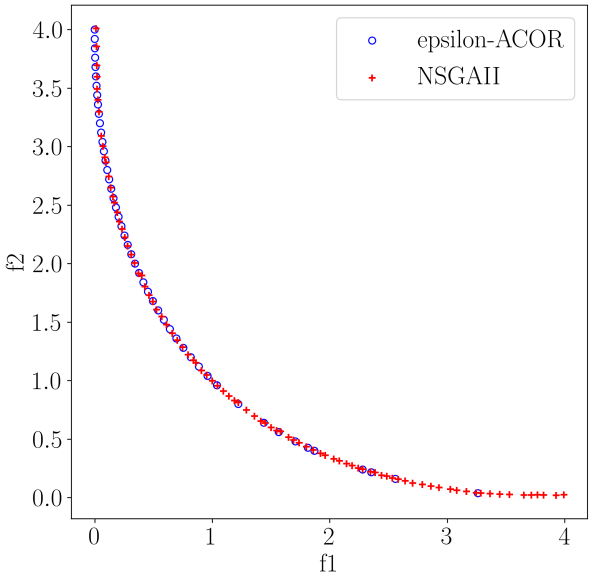

Figure 2.18: Schaffer function 1

To comment the results obtained in general, we can state that ϵ-ACO$_\mathrm{R}$ is able to deal efficiently with part of bi-objective problems, offering similar performances compared to NSGAII. For more complex problems, like ZDT functions 4 and 6, some issues remain, and NSGAII clearly outperforms ϵ-ACO$_\mathrm{R}$.

Lack of control on the number of solutions

If an exact method was used, the optimizer would find at each iteration a Pareto-optimal solution. The problem is that, with metaheuristic, the optimizer can have high variability during the solving. For example, if the optimiser is stuck in a local optimum, then it could return a dominated solution compared to the actual Pareto set. If the user desires n points for the Pareto set, there is no way to guarantee that ϵ-ACO$_{\mathrm{R}}$ would return n non-dominated solutions. It is a huge drawback, that is represented in Figure 2.16. From the 50 points requested, only a few would remain in the Pareto front.

Heterogeneity of the density of the set of solutions

A second drawback is that, with this simple version of ϵ-constraint, the Pareto-set can be not uniformly spread. An illustrative example is given with SCH1 function in Figure 2.18. The problem is that, depending on the topology of the problem, an increment of first objective function can be very different from an increment of the second objective function. It can give, for example, solutions that are not uniformly spread along the Pareto set. One technique that could help to solve the problem is a kind of "back and forth" method: if the problem is solved from f_1 to f_2, then at the end of the solving, the problem would be solved the other way around, so from f_2 to f_1.

Chapter 3

Model

3.1 Literature review

The objective of the case study is to analyse the optimal deployment for the hydrogen network in Belgium. To do so, the formulation of a relevant mathematical model is then required.

Traditionally, the design of hydrogen supply chain (HSCD) is optimised from financial perspectives, by minimizing the total cost of the system. This cost can be either annualized or considered over multiple time steps. Other considerations are less often considered in the analysis. For example, the CO_2 emissions of the supply chain could be minimized simultaneously with the costs. Indeed, today hydrogen is largely produced by SMR, the most economic option that exists. Other less polluting technologies, like electrolysers, appear on the market, but are much more expensive. Financial and environmental considerations are then antagonist, and the analysis of the trade-off between the two is the core of this master thesis.

The model that we consider is a model fixed in time, with only one time step, with both objectives (total cost and CO_2 emissions) that are annualized. It is composed of a finite set of nodes $\mathcal{N}$, composing the spatial distribution of the problem. Each node is associated to a given demand in hydrogen, that must be satisfied. The optimal design that allows to satisfy this given demand is what must be returned by the optimiser.

Storage being not considered, this leads to a three echelons supply chain: energy source-production-transport. From a set of input carriers (like methane, electricity, ...) hydrogen can be produced by conversion technologies. The produced hydrogen can then be either supplied locally, either conveyed through transport technologies to the nodes of interest. The solution describes the location and sizing of production and transport technologies, minimizing the cost and environmental impact.

Here under can be seen a graphical summary of the superstructure of the model. The

formal description of the model is explained in detail in section section 3.2. Finally, the whole set of notations can be found in Appendix B.

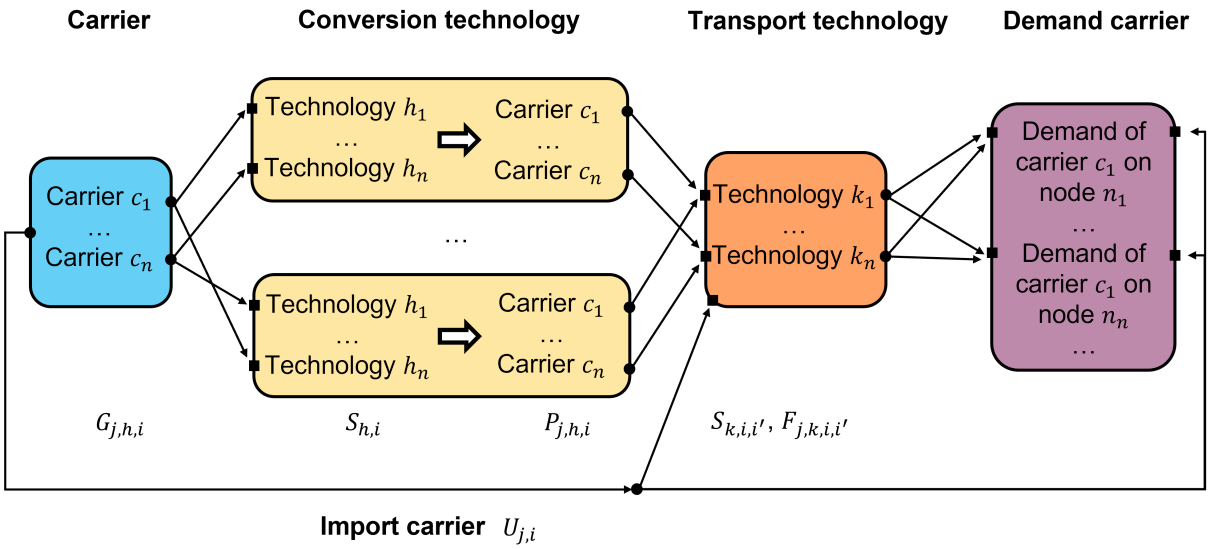

Figure 3.1: Superstructure of the hydrogen supply chain

3.2 Model formulation

3.2.1 Objective functions

Two objective functions are simultaneously minimized: annual cost and emissions. Both are computed over the year, i.e. a total of 8760 hours. The solution is then expressed as:

$$\min_{\mathbf{x}}[\mathrm{C_{tot}}(\mathbf{x}), \mathrm{GWP_{tot}}(\mathbf{x})] \tag{3.1}$$

The total annual cost ($\mathrm{C_{tot}}$) in €/year is expressed as:

$$\mathrm{C_{tot}} = \sum_{i\in\mathcal{N}}\sum_{h\in\mathcal{H}} \tau_h \mathrm{C_{inv}}(S_{h,i}) + \mathrm{C_{op}}(G_{h,i}) + \sum_{i\in\mathcal{N}}\sum_{k\in\mathcal{K}} \tau_k \mathrm{C_{inv}}(l_{k,i,i'}, S_{k,i,i'}), \tag{3.2}$$

It is distributed between conversion technologies $h \in \overline{\mathcal{H}}$ and transport technologies $k \in \overline{\mathcal{K}}$. Investment costs $\mathrm{C_{inv}}$ take into account the size of the technology in MW and for transport technologies the distances are also considered. Operational costs $\mathrm{C_{op}}$ are only considered for conversion technologies and depend on the input flow of carriers, imported for a given price in €/MWh. Investments costs are annualized with factor τ, taking into account the expected lifetime of a given technology and the discount rate for investment i_{rate} :

$$\tau(h) = \frac{i_{\mathrm{rate}}\ (i_{\mathrm{rate}}\ +1)^{\mathrm{lifetime}(h)}}{(i_{\mathrm{rate}}\ +1)^{\mathrm{lifetime}(h)} - 1} \quad \forall h \in \mathcal{H} \tag{3.3}$$

The total annual emissions of CO_2 (GWP) in tons/year are expressed as:

$$\mathrm{GWP} = \sum_{i\in\mathcal{N}}\sum_{h\in\mathcal{H}} \mathrm{GWP}_{\mathrm{op}}(S_{h,i}, G_{h,i}) + \sum_{i\in\mathcal{N}}\sum_{k\in\mathcal{K}} \mathrm{GWP}_{\mathrm{op}}(l_{k,i,i'}, S_{k,i,i'}), \tag{3.4}$$

Emissions related to construction of technologies are neglected, considering only emissions occuring during operational time of the technology. For conversion technologies it is dependant of the input flow of carriers, and for transport technologies the distances and the size of the technology expressed in MW are taken into account.

3.2.2 Constraints

In the following subsections the constraints of the optimization problem are described. These constraints were already implemented in the algorithm provided by the iMMC.

Mass balance

For all carriers $j \in \mathcal{J}$, the corresponding energy balance must be satisfied in all nodes $i \in \mathcal{G}$:

$$\begin{aligned}&\sum_{h\in\mathcal{H}}(P_{j,h,i} - G_{j,h,i}) + \sum_{k\in\mathcal{K}}\sum_{i'\in\mathcal{G},i\neq i'} (F_{j,k,i',i} - f_k(F_{j,k,i',i}, l_{k,i,i'}) - F_{j,k,i,i'}) + \\ &+ U_{j,i} - V_{j,i} - d_{j,i} = 0.\end{aligned} \tag{3.5}$$

In the previous equation:

- $\sum_{k\in\mathcal{K}}\sum_{i\in\mathcal{G},i\neq i'} F_{j,k,i',i}$ represents the import of carrier j at node i ,
- $\sum_{k\in\mathcal{K}}\sum_{i'\in\mathcal{G},i\neq i'} F_{j,k,i,i'}$ represents the export of carrier j at node i .

Technology performance

In this section is described how the performance of the conversion and transport technologies are modeled.

3.2.3 Conversion technologies

The size of conversion technology h is bounded by the maximum potential installation allowed in node i, $s^{\max}_{h,i}$. For all conversion technologies $h \in \mathcal{H}$, for all nodes $i \in \mathcal{G}$, this is expressed as:

$$S_{h,i,t,s} \leq s^{\max}_{h,i}. \tag{3.6}$$

The size of a conversion technology is defined as the rated capacity with respect to its reference output carrier.

The performance of a conversion technology h, using carriers $j \in \underline{\mathcal{J}}_h$ as input, and producing carriers $j' \in \overline{\mathcal{J}}_h$ as output, is modeled through the function $\eta_{h,j,j'}$, which

quantifies the efficiency of technology h in converting carrier j into carrier j'. This is expressed as:

$$P_{j',h,i} = \eta_{h,j,j'}(S_{h,i}, G_{j,h,i}, P_{j',h,i})G_{j,h,i} \tag{3.7}$$

with the reference output being a non-negative quantity constrained by the installed size $S_{h,i}$ of conversion technology h in node i and the minimum load of the conversion technology. If the technology is in operation ($y_{k,i} = 1$), the flow is subject to a lower bound value different from zero, otherwise is constrained to zero independently of the installed capacity, when the technology is not operating ($y_{k,i} = 0$):

$$p_h^{\min} y_{h,i} S_{h,i} \leq P_{j',h,i} \leq S_{h,i} y_{h,i} \tag{3.8}$$

The capacity of the conversion technology h at node i can be defined as the single capacity expansion $dS_{h,i}$. The increase in size has to be at least equal to Δs_h^{min} and at most equal to Δs_h^{max}:

$$\Delta s_h^{min} z_{h,i} \leq dS_{h,i} \leq \Delta s_h^{max} z_{h,i}, \tag{3.9}$$

where the binary decision variable $z_{h,i}$ describes whether the capacity of the conversion technology h is expanded ($z_{h,i} = 1$), or not ($z_{h,i} = 0$).

3.2.4 Transport technologies

The size of transport technology k is bounded by the maximum potential installation $s_{k,i}^{\max}$ at location i. For all transport technologies $k \in \mathcal{K}$, for all connections $i, i' \in \mathcal{G}$, this is expressed as:

$$S_{k,i,i',t,s} \leq s_{k,i}^{\max}. \tag{3.10}$$

Furthermore, the flow of carrier j through transport technology k between nodes i and i' is constrained by the installed size and its minimum operation load. If the technology is in operation ($y_{k,i,i'} = 1$), the flow is subject to a lower bound value different from zero, otherwise is constrained to zero independently of the installed capacity, when the technology is not operating ($y_{k,i,i'} = 0$):

$$p_k^{\min} y_{k,i,i'} S_{k,i,i'} \leq F_{j,k,i,i'} \leq S_{k,i,i'} y_{k,i,i'}. \tag{3.11}$$

The increase in size has to be at least equal to Δs_k^{min} and at most equal to Δs_k^{max}:

$$\Delta s_k^{min} z_{k,i,i'} \leq dS_{k,i,i'} \leq \Delta s_k^{max} z_{k,i,i'}, \tag{3.12}$$

where the binary decision variable $z_{k,i,i'}$ describes whether the capacity of the transport technology k is expanded ($z_{k,i,i'} = 1$), or not ($z_{k,i,i'} = 0$).

3.2.5 Limited carrier availability

Depending on the node the carrier availability can be limited. Therefore, for each node, the import $U_{j,i}$ of carrier j in node i, used in any technology in the node cannot exceed it's maximum availability $a_{j,i}$. The limited availability of carrier $j \in \overline{\mathcal{L}}$ in node $i \in \mathcal{N}$ is expressed as follows:

$$U_{j,i} \leq a_{j,i}. \tag{3.13}$$

3.3 Implementation

Part of the implementation of the model was already provided by iMMC, able to handle only single objective optimization. It is a python implementation based on Pyomo, an open-source optimization modeling language with many optimization capabilities [27].

Classically, a model in Pyomo is composed of 4 main parts:

- The variables of the model, constituting the solution returned by the optimizer. In our case, it is composed for example of the capacities of the different production technologies, import of carriers, ... The exhaustive list of decision variables can be found in Table B.4
- The parameters that are treated as input for the model. The exhaustive list of parameters can be found in Table B.3. The data used for the parameters is described in section 4.1
- All relations defining the model, so all the equations (contraints, ...) related to the model desciption and already described in subsection 3.2.2
- The goals, or objective functions that need to be optimized, in this case total cost C_{tot} and CO_2 emissions GWP_{tot}, described in subsection 3.2.1

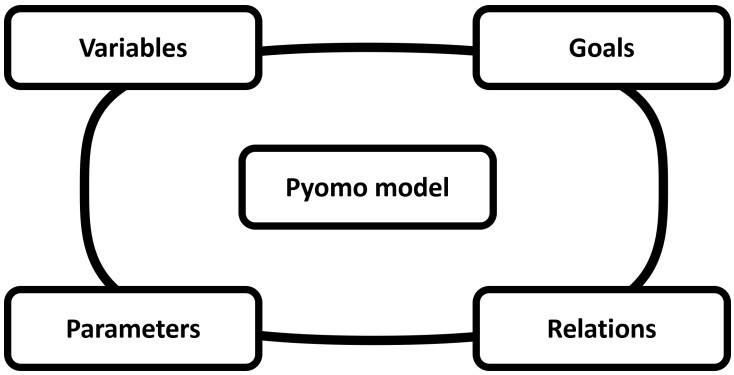

Figure 3.2: Typical model composition in Pyomo

3.3.1 Single objective formulation

Reference implementation

In a first step, two implementations were developed simultaneously for single objective optimization. First, a reference version, where the model is linearized. Mixed Integer Linear Programming (MILP) allows to use a classical ILP (integer linear programming) solver, and to use the solution as a reference to compare it with the metaheuristic. The approach is illustrated in Figure 3.3. In a first step, only two sources of non-linearities are considered: investments costs (Capex) and efficiencies of the electrolysers. More

explanations about the technology can be found in subsection 4.1.2. The linearization is achieved with a piecewise affine function (PWA). It consists of a partition of the function into local disjoint regions, each of which is associated with an affine function. [28].

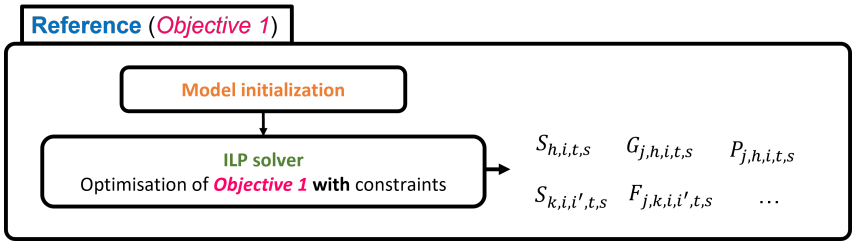

Figure 3.3: Reference implementation for single objective problems

Hybrid implementation

Secondly, a second version was implemented, with a Mixed Integer Non-Linear Programming (MINLP) formulation. It integrates the metaheuristic, allowing to handle the non-linearitities of the model without linearization. As there is a large number of decision variables and constraints, solving the problem with only metaheuristic is unrealistic: covering the whole search space would require a too high computational time. To deal with the issue, a Master-Slave architecture is adopted. In this case, metaheuristic is used as master algorithm to handle given decision variables, while the classical ILP solver is used to solve the problem by adjusting the remaining variables. A similar approach was used in [29], and the process developed for this work is represented in Figure 3.4.

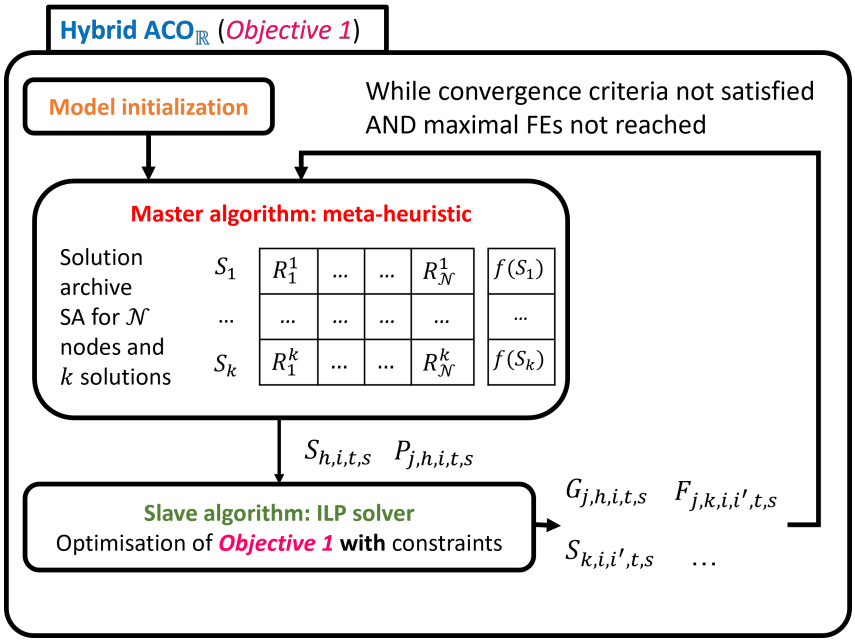

Figure 3.4: Hybrid implementation for single objective problems

In our case, metaheuristic chosen as master algorithm is ACO_{MV}. However, as only continuous variables are handled for this master thesis, only ACO_R is used. The solution archive SA creates and stores a set of k initial solutions for $\mathcal{N}$ nodes. ACO_R handles only the decision variable subject to nonlinearities, which includes $S_{h,i}$, being the capacity of conversion technology h at node i, and $P_{j,h,i}$, being the output stream of carrier j from conversion technology h at node i. Once the new set of solutions is created, the slave algorithm optimizes the objective function, for each solution in SA, with $S_{h,i}$ and $P_{j,h,i}$ fixed by the metaheuristic and adjusting the rest of the decision variables. Then, all the solutions are ranked in SA and sorted accordingly. The process is repeated, with the creation of new solutions at each iteration (see flow chart of ACO_R in Figure 2.3 for more details) until the convergence criteria is satisfied or the maximal number of function evaluation is reached.

3.3.2 Multi-objective formulation

The last step in the implementation process is to include the bi-objectivity. As developped in subsection 2.3.5, ϵ-ACO_R is the method chosen for this work. The ϵ-constraint method is placed at the top level of the algorithm, at a higher level than the single objective optimizer. It takes as input p, the number of solutions that the user desires for the pareto set. Then, the upper and lower bounds are computed, by optimizing separately the two different objectives. It means that one objective is optimized, while the second is unconstrained. The single objective optimizer can be used nearly without modification, for both the reference and the hybrid implementation. The only change is that it takes two extra inputs: a second objective, which has to be constrained by the ILP solver, and ϵ, the level of this constraint. Practically, in Pyomo, multiple objectives can be implemented, but only one at a time can be activated.

Once the extreme points of the Pareto set are determined, an increment $d\epsilon$ is computed, depending on the density of the Pareto set p. Then, the ϵ level is progressively increased by $d\epsilon$, calling the hybrid ACO_R to optimize the total cost while constraining the emissions under ϵ level. Note that it could also have been done in another order, then optimizing the emissions while constraining the costs. Reference and hybrid implementations are represented in Figure 3.5 and Figure 3.6.

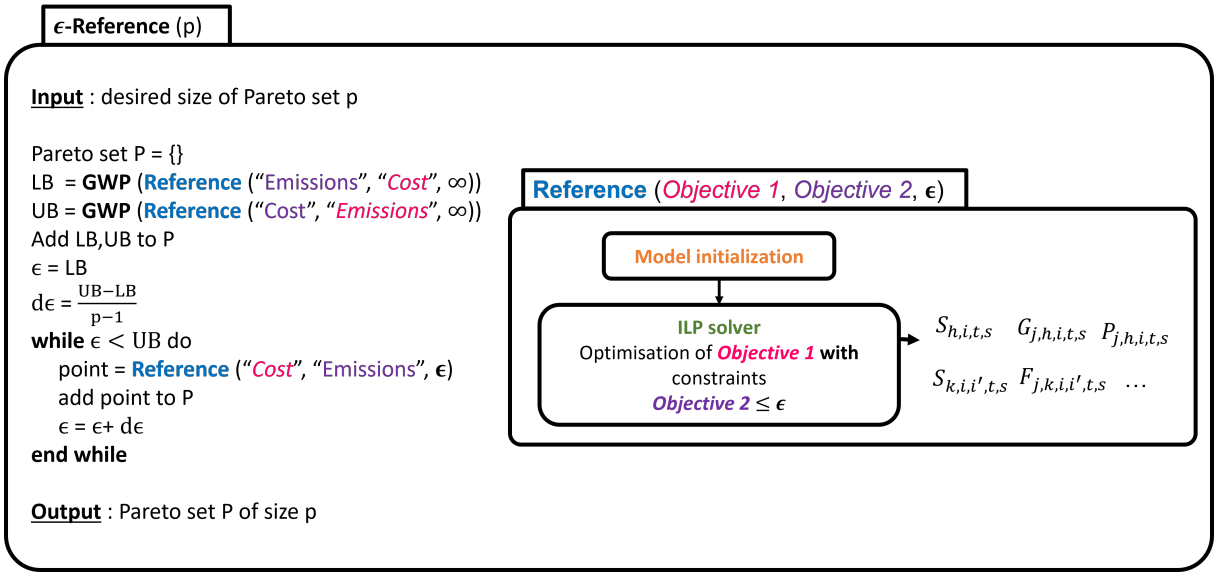

Figure 3.5: Reference implementation for bi-objective problems

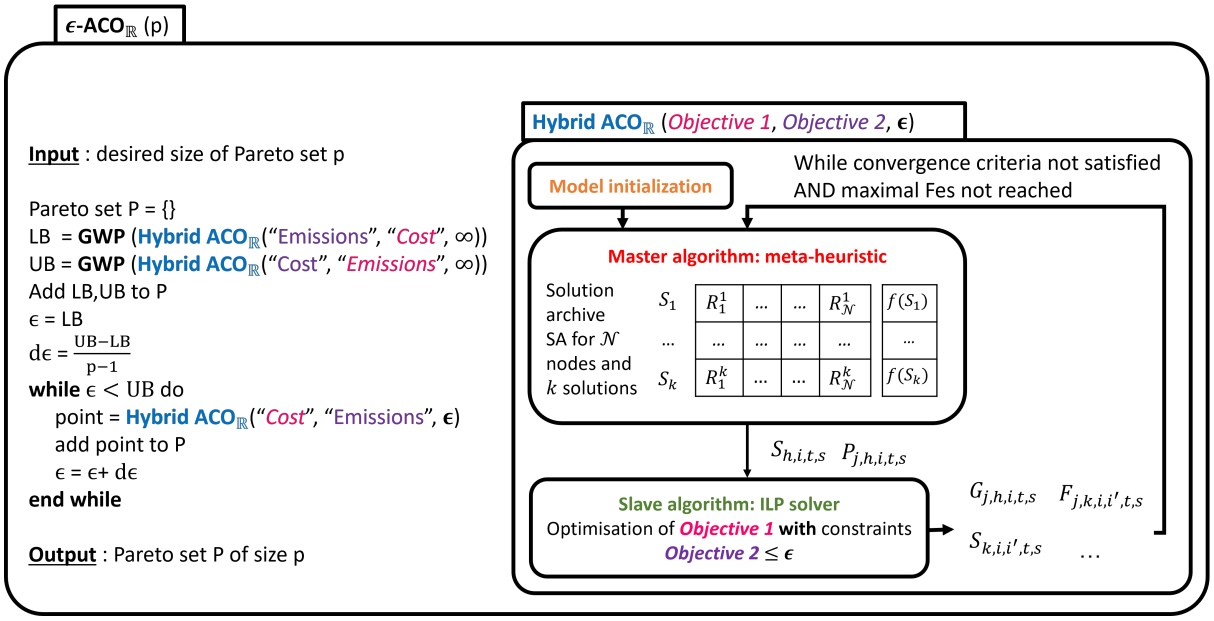

Figure 3.6: Hybrid implementation for bi-objective problems

Chapter 4

Case study

4.1 Input data

4.1.1 Demand in hydrogen

Sectors

The European hydrogen market can be divided in 3 categories, represented in Figure 4.1: merchant companies which trade hydrogen, captive producers which produce hydrogen for their direct customer or their own use and finally by-product hydrogen resulting from chemical processes [30].

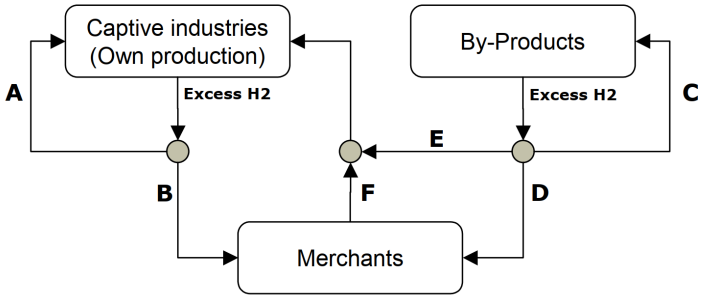

Figure 4.1: Classical organization of the hydrogen market [30]

In Belgium, the three are present in the market. In our analysis, 4 industrial sectors will be considered as hydrogen consumers: refineries, ammonia production, hydrogen peroxide production and steel industry.

Refineries

Oil refining is the largest user of hydrogen in Europe, turning crude oil into various end-user products such as transport fuels and petrochemical feedstock [31]. In refineries, most

of the hydrogen is needed for hydro-cracking and hydro-treating de-sulphurisation units, that allow to remove the impurities. Hydrogen can also be produced as by-product, from catalytic cracking in the catalytic reforming units [30]. However, the net balance depends strongly from a refinery to another, then the demand in hydrogen is computed with the actual consummption of hydrogen in considered plants.

In Belgium, there are two main actors in the refinery sector: TotalEnergies and Exxon-Mobil. Both have large facilities in Antwerp, while TotalEnergies has also a plant located in Wallonia, in Feluy.

Ammonia production

Ammonia production is the largest consumer of hydrogen in the chemical industry. Ammonia is mainly used for the production of fertilizers such as ammonium nitrate or urea (almost 80%), while the remain part is consumed in explosives, synthetic fibers and special materials industries [31]. The production process involves a synthesis of hydrogen with nitrogen, consuming around 1985 $m^3_{H_2}$ per ton of nitrogen.

$$N_2 + 3H_2 \rightarrow 2NH_3 \tag{4.1}$$

BASF, based at Antwerpen, is a Belgian leader in the chemical industry and in ammonia production, followed by Yara, with a unit at Tertre. BASF is also producing a lot of hydrogen as by-product, for example with their production of Ethylene and Styrene.

Hydrogen Peroxide production

Hydrogen Peroxide (H_2O_2) is usually produced acording to:

$$H_2 + O_2 \rightarrow H_2O_2 \tag{4.2}$$

It consumes less hydrogen than for ammonia, with a theoretical need of about 735 $m^3_{H_2}/t_{H_2O_2}$. The production in Belgium, exclusively covered by Solvay, is less important than the ammonia production but not negligible.

Steel industry

All previous sectors are currently using hydrogen in their production process. Yet, hydrogen can also be used to decarbonize other activities, that traditionally are not using hydrogen. A good example is the steel industry, still very present in Belgium, even if on a downward slope since a few years.

In Belgium, two main technologies are present for steelmaking. In the largest majority, electric arc furnaces, where steel is molten by electric arcs, and also Blast Furnaces associated to Basic Oxygen Furnace. Hydrogen can be used on BF-BOF road as an auxiliary reducing agent, called H2-BF, illustrated in Figure 4.2. It reduces the amount of coal needed and only forms water after reacting with iron ore instead of carbon dioxide [32].

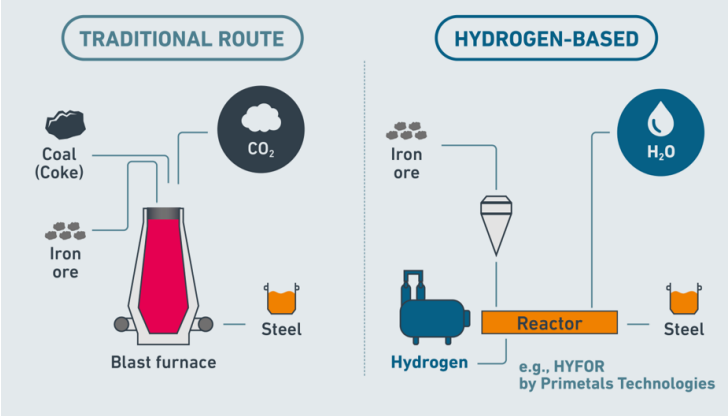

Figure 4.2: H2-BF road to decarbonize steel industry [33]

The global strategy to decarbonize steel industry is to ally the electric arc furnaces, that does not emit carbon dioxide if the electricity comes from renewable sources, and H2-BF [34]. In Belgium, most of steel producers are based on electric arc furnaces ; one single production site, located in Gent, uses BF-BOF road [35]. In our scenario, we will only consider a potential switch to H2-BF on ArcelorMittal site. The demand in hydrogen is estimated at around 55 kg_{H_2}/ton_{steel} [32].

Demand location

The next step is to compute the demand of hydrogen for each production plant. For ammonia production, hydrogen peroxide or steel, the demand is estimated with the mass of hydrogen needed to produce 1 ton of product, summarized here under:

- Ammonia: 0.175775 t_{H_2}/ton_{NH_3}[30]
- Hydrogen Peroxide: 0.065415 $t_{H_2}/ton_{H_2O_2}$[30]
- Steel: 0.05 t_{H_2}/ton_{steel} [32]

Knowing the output rate of each plant individually, a given demand in hydrogen is computed. Note that for ammonia and hydrogen peroxide, hydrogen is already produced today to satisfy this need, while for steel it is a prediction to decarbonize the industry.

Concerning refineries, there is no direct relationship between the output rate of oil and hydrogen needed, since it depends strongly from a refinery to another. Then, the demand was estimated with the actual production rate of hydrogen intended for refineries. From

the data in [30] and [36], we translate the yearly production into hydrogen demand. All the data used in different sectors is summarized in Table 4.1.

Sector	**Plant**	**Location**	**Production [kt/y]**	**Demand H2 [$10^3 m^3$/d]**	**Demand H2 [TWh/y]**
Refineries	TotalEnergies	Antwerp	/	652.2142857	0.706004521
	Exxon	Antwerp	/	2189.214286	2.369765913
	Total	Feluy	/	240	0.259793581
NH3	BASF	Antwerp	NH3: 690	/	4.041480625
	BASF	Antwerp	/	791	0.856236345
	Yara	Tertre	NH3: 400	/	2.342887319
H2O2	Solvay	Anvers	H2O2: 230	/	0.501348229
	Solvay	Jemeppes sur Sambre	H2O2: 90	/	0.196179742
Total					11.27369627
Steel	Arcelor Mittal	Gent	Steel: 5000	/	8.33056222
Total					19.60425849

Table 4.1: Industrial demand of hydrogen in Belgium

	Sector	**Plant**	**Location**	**Prod H2 [$10^3 m^3$/d]**	**Prod H2 [TWh/y]**
SMR	Refineries	TotalEnergies	Antwerp	337	0.364793487
		Exxon	Antwerp	1130	1.223194778
		TotalEnergies	Feluy	240	0.259793581
	Ammonia	BASF	Antwerp	4524	4.897109005
	H2 Peroxyde	Solvay	Antwerp	2180	2.359791696
	Total			8411	9.104682547
By-product	Refineries	TotalEnergies	Antwerp	744	0.805360102
	Ethylene, Styrene	BASF	Antwerp	791	0.856236345
	Chlorinated Solvents	Tessenderlon	Hasselt	227	0.245721429
	Chlorinated Solvents	Solvay	Antwerp	238	0.257628635
	Total			2000	2.16494651
Total				18822	11.26962906

Table 4.2: Industrial production of hydrogen in Belgium

To sum up, total existing demand of hydrogen corresponds to 11.27 TWh/year, and if we consider predictions for steel industry, the total raises to 19.6 TWh/year. Concerning

the existing demand, we can check if the demand estimated with output rates of product (ammonia, hydrogen peroxide, ...) corresponds to the existing production of hydrogen in Belgium. The production is decomposed in 2 groups: merchant production, based on steam methane reforming, and by-product production, coming for example from hydrocracking, ethylene or styrene production, ... By adding the production by SMR and the by-products, the total production of hydrogen is of 11.269 TWh/year. It corresponds to the previous computed demand of hydrogen (excluding steel industry), equal to 11.273 TWh/year.

A nodal representation is then designed for the case study. To avoid useless complexity, plants closer than 5 km from one to another are considered as a single node. For example, the four plants in Antwerp are simplified in two distinct nodes instead of four. In total, it results in 6 nodes, spread over the territory. The spatial distribution of the nodes is represented in Figure 4.3, and the computed demand associated to each node is represented in Figure 4.4 and in Table 4.3.

To sum up, the set of 6 nodes is associated to spatial coordinates and a given demand in hydrogen. The other characteristics related to the nodal distribution described in the model formulation (technology availability, ...) are discussed in the following sections.

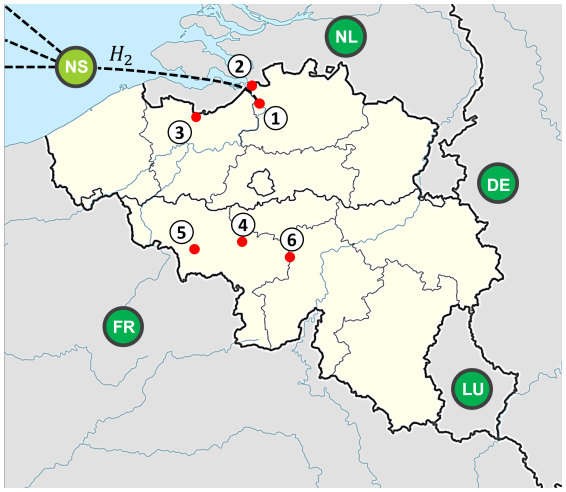

Figure 4.3: Nodal representation of the case study

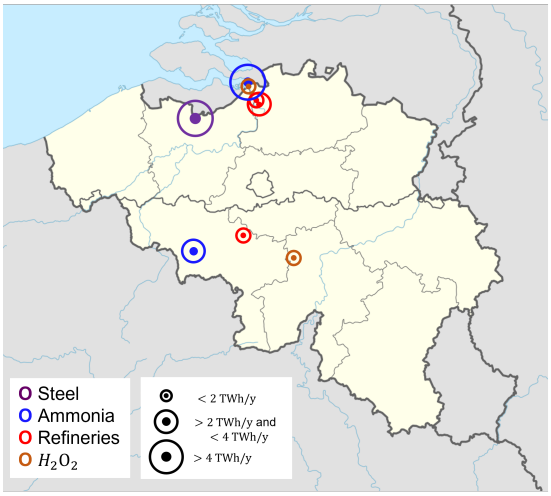

Figure 4.4: Industrial hydrogen demand in Belgium per node

4.1.2 Conversion technologies

Two conversions technologies are considered in the set $\mathcal{H}$, allowing the conversion of input resources into hydrogen.

Index	Node	Demand [TWh/y]
1	Total-Exxon ANTW	3.076
2	BASF-Solvay ANTW	5.391
3	Arcelor GHENT	8.330
4	Total FELUY	0.259
5	Yara TERTRE	2.342
6	Solvay JSS	0.196

Table 4.3: Hydrogen demand in Belgium per node

Steam Methane Reformers

SMR is the most widespread technique for hydrogen production, responsible of more than 50% of total production of hydrogen [37]. In Belgium, it is responsible for most of the production, and it remains the least expensive method for hydrogen production available in terms of its capital cost [38].

Hydrogen is produced by having a reaction between hydrocarbon and water. Natural gas is the most used as feedstock. The steam reforming (SR) reaction produces 3 moles of hydrogen per mode of methane. Additionally, via the water gas shift reaction (WGSR), additional hydrogen is released by reaction of water with the carbon monoxide generated:

$$CH_4 + H_2O \rightleftharpoons CO + 3H_2 \tag{4.3}$$

$$CO + H_2O \rightleftharpoons CO_2 + H_2 \tag{4.4}$$

Optimal SMR reactor operates within a temperature range of 800 °C to 900 °C at medium pressures of 20-30 bar. The reaction is conducted in multitubular packed bed reactors, consisting of an array of long and narrow tubes which are situated within the combustion chamber of a large industrial furnace. Inside the tubes, a mixture of steam and methane is put into contact with a nickel catalyst [39]. With an efficiency varying between 65% and 75% [38], an average efficiency of 70% is adopted for all the plants. The process flow of typical steam reforming plant is represented in Figure 4.5.

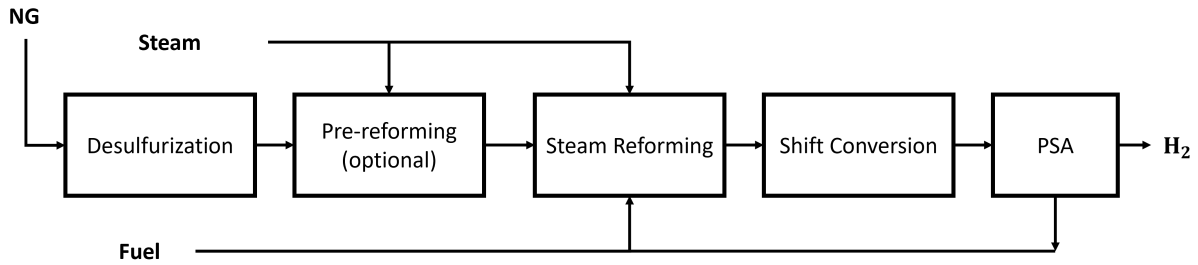

Figure 4.5: General process flow of a typical steam reforming plant [38]

In the absence of Carbon Capture and Storage (CCS), the process releases carbon dioxide to the atmosphere: hydrogen produced is called "grey" hydrogen. If CCS is present, hydrogen has the denomination of "blue" hydrogen. However, to simplify the problem, CSS installation on operating SMR plants is not envisaged in this case study. As the possibility to install new units of SMR is neglected, only allowing to use existing plants, no capital costs are associated to SMR.

Electrolysers

Electrolysis consists in splitting the water molecules into gaseous hydrogen (H_2) and oxygen (O_2) using electricity (direct current). This electrochemical reaction occurs when an external voltage is applied to a device called an electrolyser. Water electrolysis is the combination of two half reactions, which take place at the cathode and at the anode [40].

$$2\mathrm{H_2O(I)} \rightarrow 2\mathrm{H_2(\ g)} + \mathrm{O_2(\ g)} \tag{4.5}$$

The electrochemical generation of hydrogen is an available technology from the end of the 19th century. Yet, around 4% of total hydrogen produced in Europe is produced by electrolysers [6]. If the electricity required by the process comes from renewable sources, the hydrogen produced is called "green hydrogen". Two main different technologies of electrolysers exist today:

- Alkaline Electrolysis (AEL) which is the most mature technology. The electrolyte used is a liquid solution of water with 30% of Potassium Hydroxide (KOH). The hydrogen produced can be contamined by water, oxygen or electrolyte in itself.
- Polymer electrolyte membrane (PEM) electrolysis, where the electrolyte is solid with a proton-conducting polymer membrane, and not liquid anymore as in AEL. In contrast to the alkaline technology that allows ions OH- migration, the polymer membrane is hermetic to anions as well as oxygen and hydrogen [40]. It allows a production of hydrogen slighty purer. Only PEM technology is included in this analysis.

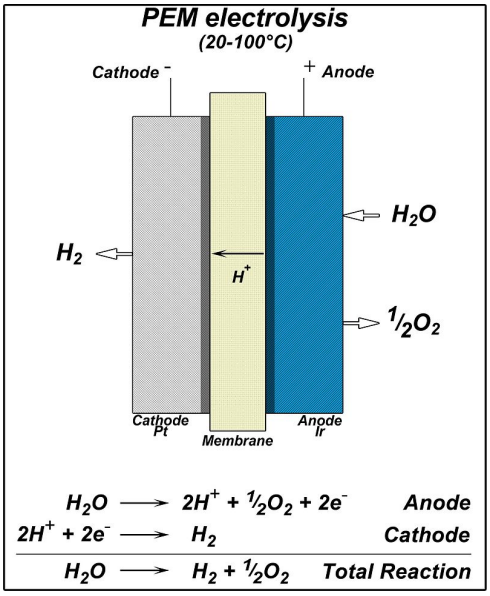

Figure 4.6: Diagram of PEM electrolysis reactions [41]

The only source of non-linearities in the model comes from the PEM electrolysis. First, the investments costs that are non-linear for capacities between 0 and around 100 MW. Secondly, in conversion efficiencies, but only for small output volumes under 100 MWh, which is very small compared to the national scale of the problem. Both non-linear distribution, but also the PWA breakpoints, used in the classical reference linearized version, are represented in Figure 4.7 and Figure 4.8.

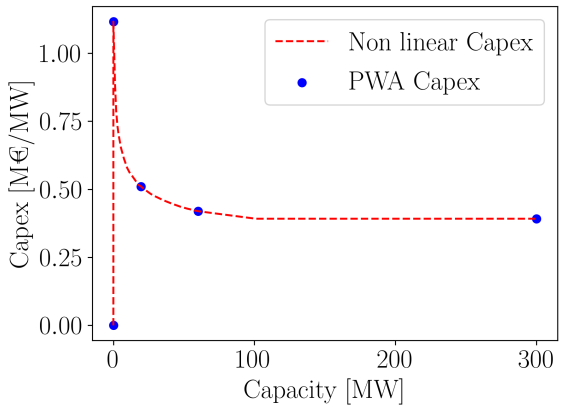

Figure 4.7: Capex of PEM

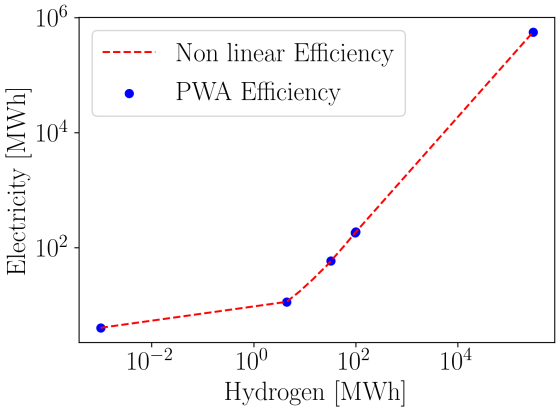

Figure 4.8: Conversion efficiency of PEM

In the case study, we consider that all the existing plants are SMRs, and that there is no possible ways to build new SMR production units. Electrolysers have a limited availability of 300MW per node, and are available everywhere. For all technologies, the discount rate is set at 1.5%. For electrolysers, the installation and operational costs are considered, while SMRs only include the operational costs, since all the units are already

installed. The lifetime of electrolysers is set at 20 years [41].

	Availability [MW]	
Nodes	Electrolysis	SMR
Total-Exxon ANTW	300	181.27
BASF-Solvay ANTW	300	828.03
Arcelor GHENT	300	0
Total FELUY	300	29.65
Yara TERTRE	300	0
Solvay JSS	300	0
Total	1800	1039.35

Table 4.4: Availability Electrolysis and SMR per node

4.1.3 Carriers

Electricity

Green electricity can be imported theoretically either from the national grid, either from neighbouring countries: France, Germany, Netherlands or Luxembourg. According to the data of [42], presented in Figure 4.10, net green potential of Belgium, so green electricity available for electrolysis after self-consumption of electricity, is negative. Then, the total available green electricity, for all the nodes, is the sum of available green electricity by the four neighbors, equal to 1060 TWh/y. The available green electricity is the total green potential, minus the self consumption in electricity and the consumption of electricity required for supplying the total hydrogen demand with electrolysis.

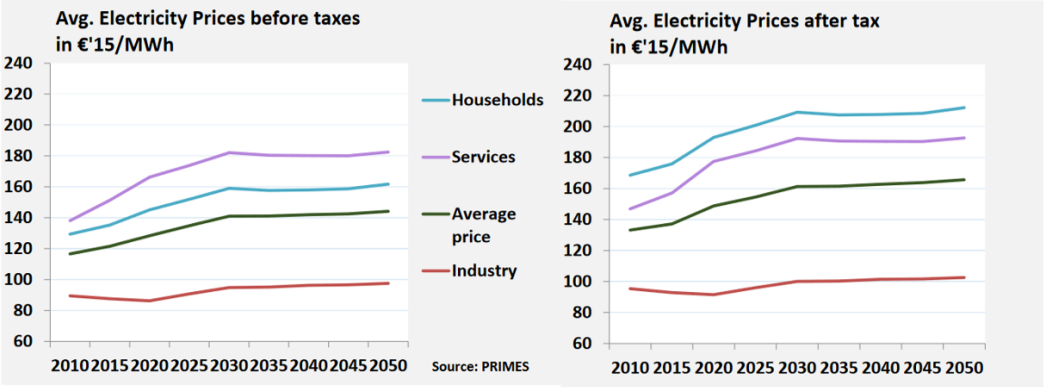

Figure 4.9: Average electricity prices in the European Union per sector [43]

From the Figure 4.9, we can extract the price of import of electricity, estimated at 100 €/MWh, that we simplify to be equal among all the neighbors. It is a projection for

the period of 2030-2035, considering an average industrial relail price of electricity in the European Union, including taxes. Since we envisage a transition to green hydrogen up to 2050, the transition must begin from 2030. That is why we consider the prices from 2030 rather than 2050.

Country	Belgium	France	Luxembourg	Germany	Netherlands
Availability [TWh/y]	0	917	0	0.69	142.2

Table 4.5: Availability of imported green electricity from neighboring countries of Belgium

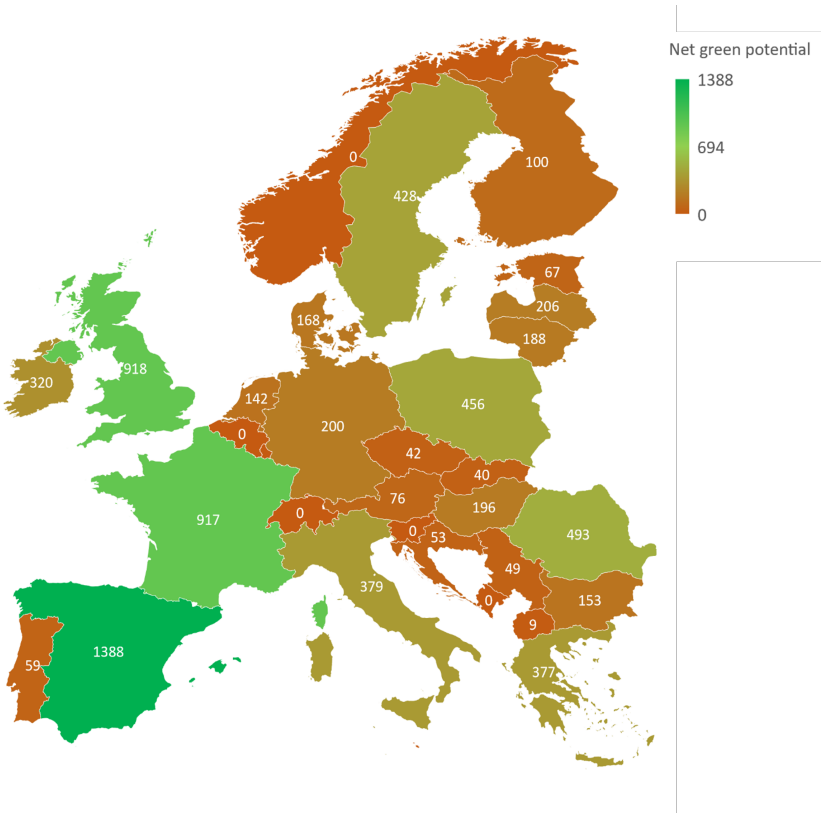

Figure 4.10: Excess or deficit of net potential of green electricity for the European countries after self-consumption [42]

Hydrogen

Hydrogen can be produced onsite from the two previously cited conversion technologies, but we also consider the possibility to import it from abroad. Indeed, some countries have very large potential for renewable technologies (Chile, Marocco, ...) and have as objective to produce and export green hydrogen in large quantities. The import of hydrogen is realized via the North Sea and the port of Antwerp, with infinite availability

and for a given price. The sea routes and the different exporting countries are illustrated in Figure 4.11. The emissions linked to the transport by shipping are neglected, a quite strong assumption justified by a probable hydrogen use for fuelling the ships.

Figure 4.11: Sea routes of imported hydrogen[40]

In Table 4.6, we can see the expected prices to import hydrogen from different countries. In the 2030-2035 period, the average sum for cost of imported green hydrogen is of 102 €/MWh [40]. This price includes for example the production of electricity, the Capex and Opex of production, the transport via pipelines, shipping, ...

Country	Australia	Chile	Oman	Marocco	Best of Iberia	North Sea
Price [€/MWh]	124.85	102.44	93.34	89.97	105.20	95.10

Table 4.6: Price prediction of imported hydrogen by 2030-2035 in Belgium [40]

Natural gas

Natural gas is required for SMR. We consider that for 1 MWh of hydrogen produced by SMRs, 0.217 tons of carbon dioxide are released in the atmosphere. The availability of the resource is not constrained.

Different estimations for the price of import of natural gas in Belgium 2030-2035 can be found in [44] and are shown in Table 4.7. It is decomposed in multiple scenarios coming from different reports, each one associated to a reference, low and high cases. The final average price is of 37.1 €/MWh.

	Price [€/MWh]		
Scenario	REF	Low	High
Background Report	49,3	45,1	49,8
IEA 450 Scenario	39,2	36,0	39,5
IEA new Policies	42,9	39,3	43,1
EU-Long Term	35,2	32,3	35,3
IEA Current Policies	46,4	42,3	46,6
JRC -Ref	30,6	28,1	30,9
JRC - High	40,1	37,3	40,6
JRC - Low	20,3	19,1	20,3
Average	38,0	34,9	38,3
Total average	37,1		

Table 4.7: Price prediction of natural gas by 2030 in Belgium [44]

Water

Water is an input carrier required for electrolysis and SMR. It is considered as unlimited and the cost of water is neglected.

In Table 4.8, the availability, cost and emissions associated to each carrier considered are summarized.

Carrier	Availability [TWh/y]	Cost [€/MWh]	Emissions [ton_{CO_2}/MWh]
Electricity	1060	100	0
Hydrogen (from North Sea)	∞	102	0
Natural gas	∞	37	0.217
Water	∞	0	0

Table 4.8: Attributes of the carriers

4.1.4 Transport technologies

Pipelines

In the next decades, both new pipelines and utilization of existing infrastructure (re-qualification of pipelines transporting for example natural gas) are viable options for the transport of hydrogen [45]. However, the re-qualification of existing infrastructure is out of the scope of this work, focusing on the design of new network. Different sizes of pipelines exist, from 50 cm of diameter to 127 cm for existing gas European network. 91- and 127-cm can transport respectively around 7- and 13-GW of hydrogen per pipeline, mainly for long distance transport [46]. In our analysis, the maximal transport capacity of pipelines

is chosen as 7 GW. There are no emissions associated to the transport of hydrogen though pipelines. The emissions related to the construction of new pipelines are neglected. The lifetime is estimated at 50 years.

Trucks

Trucks is the second option considered in this work for the hydrogen transport. The trucks that haul gaseous hydrogen are called tube trailers. Gaseous hydrogen is compressed to pressures of 180 bar or higher into long cylinders which are stacked on the trailer that the truck hauls [47]. Trucks are a viable option for smaller volumes of hydrogen: we consider a maximal capacity of 14 MW per connection [48]. On the contrary, pipelines are a more economic option for both larger capacities or more important distances. As a simplification, we state that pipelines cannot be installed for capacities of under 14 MW, to be consistent with the trucks.

Attribute	Units	Pipelines	Trucks
Minimal built capacity	MW	14	0
Maximal built capacity	MW	7000	14
Flow loss	1/km	0 [49]	0.00012 [49]
Cost	€/km/MW	4100 [49]	13000 [49]
Emissions	ton_{CO_2}/km/MWh	0 [49]	$4.2 \cdot 10^{-6}$ [49]

Table 4.9: Attributes of transport technologies

4.1.5 Summary

The summary of the model used for the case study is presented in Figure 4.12.

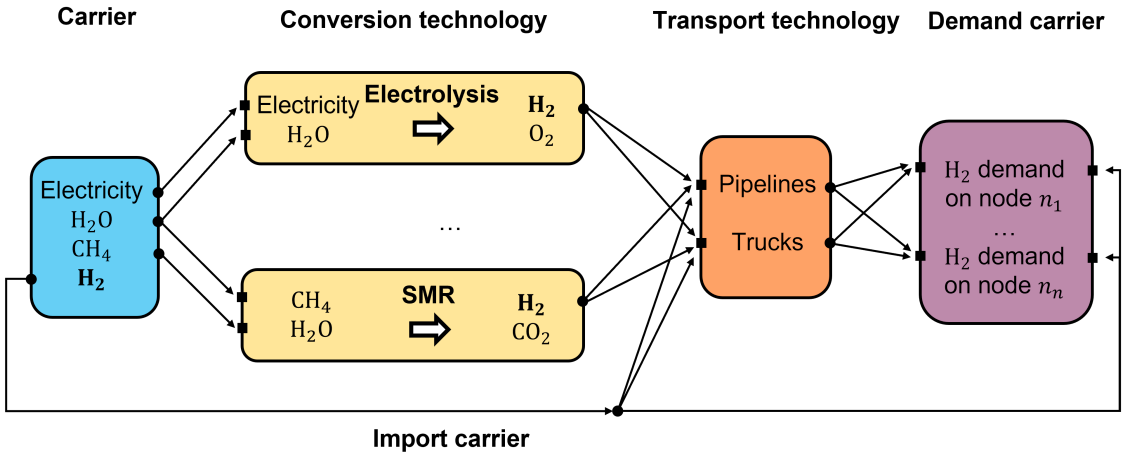

Figure 4.12: Hydrogen supply chain of case study

4.2 Results

In this section the results of the analysis are presented. It allows to compare the different implementations of the tool described in section 3.3 to the case study documented in section 4.1.

4.2.1 Reference case for 2030-2035

The results present an analysis of the trade-off between cost and CO_2 emissions and the comparison between hybrid and reference implementation. In all the tests, 8 points are evaluated in order to represent the Pareto front. The maximal number of function evaluation is set at 10^6.

First, in Figure 4.13, is presented the Pareto front of the set of 8 points composing the solution, for both the hybrid metaheuristic algorithm and the simplified linearized model. We can observe that the hybrid implementation offers the same performances than the linearized version, and the fact that no electrolysis unit is built in this scenario explains the linearity of the Pareto front, since the only non-linearities of the model are present in installation costs and efficiency of electrolysis plants. The minimal and maximal relative errors in term of cost between MILP and MINLP formulations through the Pareto front are respectively $7 \cdot 10^{-13}$ and $6.9 \cdot 10^{-4}$, which is more than acceptable. We can conclude that the hybrid version, for a higher computational cost, offers at least the same quality of solutions than the classical solver.

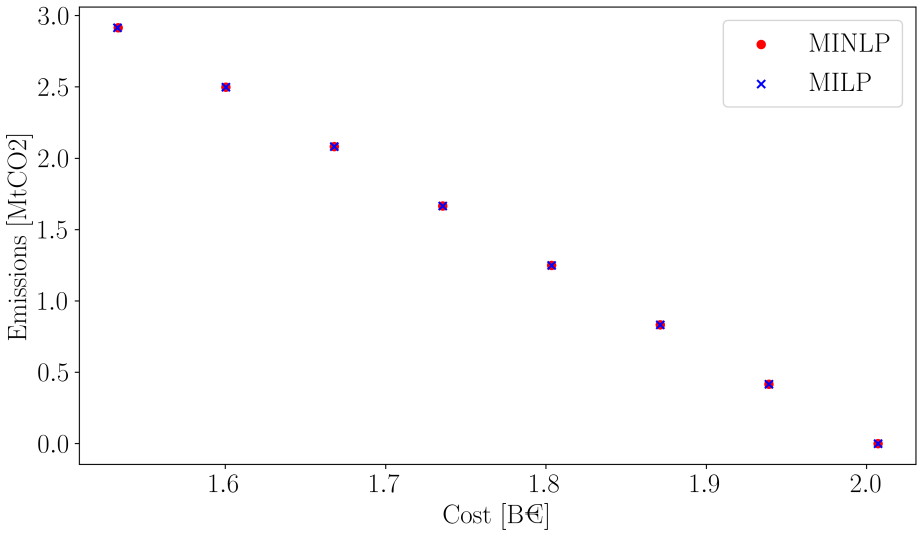

Figure 4.13: Pareto front comparison between hybrid metaheursitic (MINLP) and linearized (MILP) implementations

We can also observe that cutting the actual 2.9 Mt of CO_2 emissions to zero can be achieved but with a cost augmentation of 30% compared to the optimum in terms of costs.

To understand the changes through the Pareto set, the evolution of the sources of hydrogen (produced or imported) is presented in Figure 4.14, with the relative contributions of electrolysers, SMRs and imported hydrogen. Operating SMRs are progressively removed and replaced by imported green hydrogen, neglecting electrolysis deployment. In the case of Belgium, it is not profitable to develop new electrolysis plants onsite. It is due to very competitive prices of imported green hydrogen compared to the average price of electricity in European Union, and the assumption that imported hydrogen has the same zero-carbon impact than locally built electrolysers.

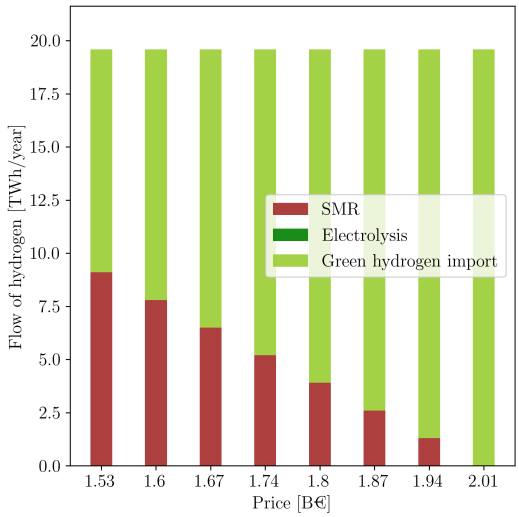

Figure 4.14: Mix of hydrogen produced/imported through the Pareto front

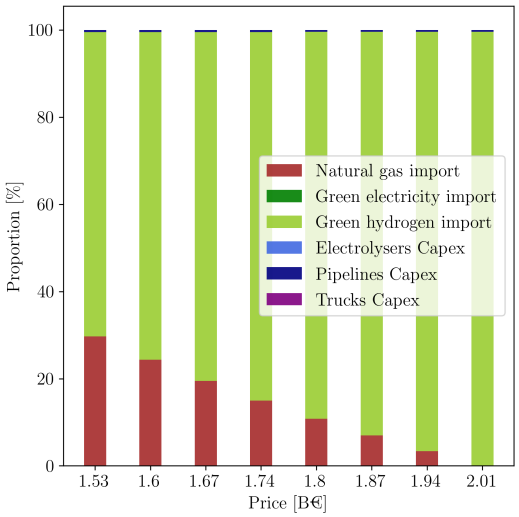

Figure 4.15: Breakdown of total cost through the Pareto front

The decomposition between investment and operational cost is presented in Figure 4.15. The construction of pipelines represents a very negligible impact on the total cost compared to the import of resources. It is also due to the annualization of the costs and the long lifetime of pipelines. Since the SMR units are already in place, they do not represent any investment costs.

Finally, the network representation of the two extreme solutions of the Pareto set is represented in Figure 4.16 and Figure 4.17, associated to minimal cost and minimal emissions. It includes both the spatial distribution of produced or imported hydrogen and the hydrogen flows through different nodes. The flow of hydrogen is represented as a percentage of the total demand. In the set of solutions, hydrogen is imported from the port of Antwerp and is transported through pipelines to the other plants, progressively replacing existing infrastructure based on SMRs.

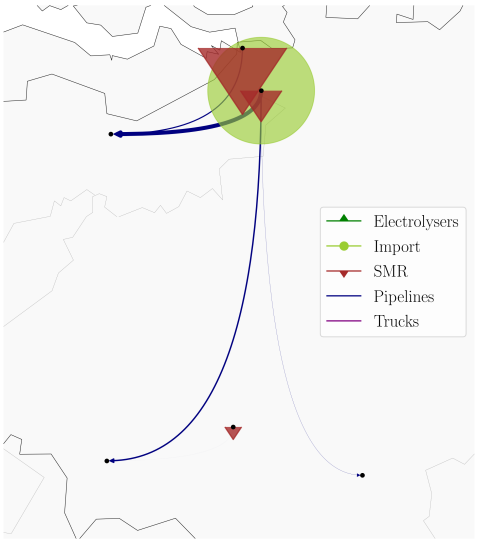

Figure 4.16: Optimal network minimizing the total cost

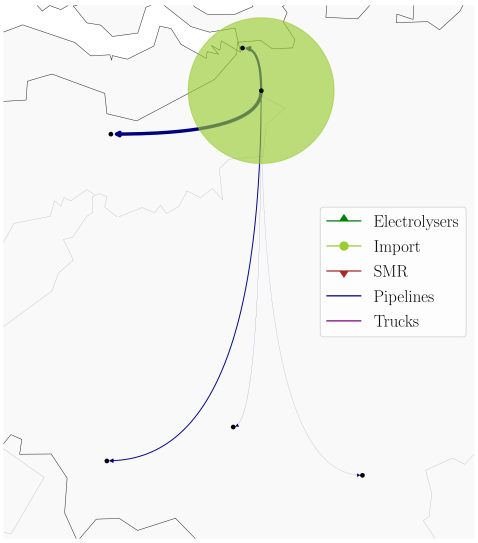

Figure 4.17: Optimal network minimizing the emissions

Theses results remain very trivial results: no unit of electrolysers is installed, mainly due to high prices for green electricity, which cannot be produced onsite in Belgium due to a zero green electricity potential.

4.2.2 Extra cost of electrolysers

Apart from financial perspectives, there could be advantages to build a local green hydrogen economy: the total energetical dependence from other countries, far from European Union, could be seen as a drawback for the transition to green hydrogen production. If a decision maker imposes to develop industrial electrolysis in Belgium, what would be the difference in terms of cost with the optimal reference solution? In other words, what would be the price to pay to make electrolysis in Belgium a reality ?

In this section, the financial gap between optimal reference case and solutions including local electrolysis is analysed. To do so, different values of minimal total capacity of electrolysers are imposed. Only the total capacity over the country is constrained, and not the location, allowing to keep an optimal design even with this additional constraint. The objective is to see the difference in term of cost between the different Pareto fronts.

The different steps imposed for the capacities are 60, 300, and 1000 MW. The different corresponding Pareto fronts are represented in Figure 4.18. As expected, the cost is increasing with the total capacity imposed. In Table 4.10, the relative increase of the total cost is summarized for each level of capacity imposed. This increase is an average value measured along the whole Pareto front, a simplification justified by the linearity of

the curve, and the increase is compared to the reference case solution.

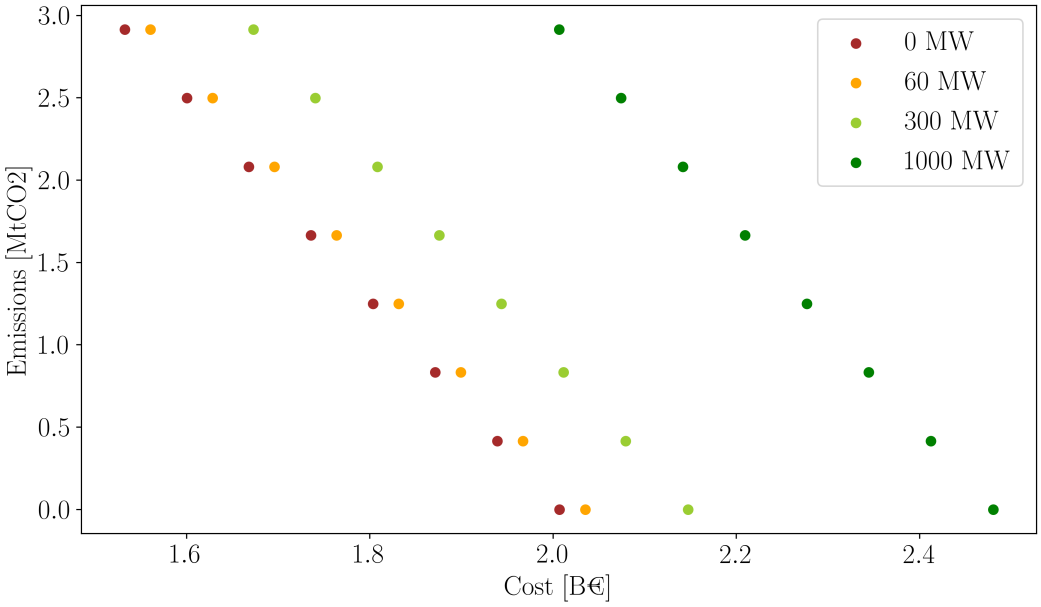

Figure 4.18: Pareto fronts with different total capacities of electrolysers imposed

Capacity [MW]	Increase of cost [%]
60	1.6
300	8
1000	27

Table 4.10: Average relative increase of cost in % through the Pareto front, compared to the reference case solution

In the next figures, the network representation of two situations is represented, associated to a total capacity of electrolysers of respectively 300 and 1000 MW. It can be observed that electrolysers are installed first in Wallonia, on plants that are further from port of Antwerp, avoiding to build longer pipelines. If the capacity increases to 1000 MW, then the electrolysers are spread all over the country. As in reference solution, SMRs are progressively replaced, here by a mix of electrolysis and imported hydrogen.

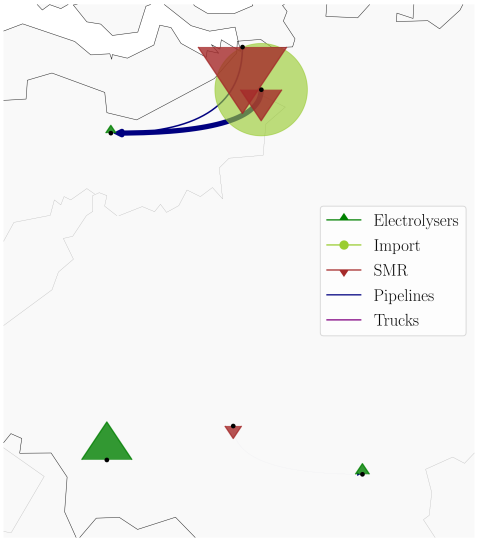

Figure 4.19: Optimal network minimizing the total cost, with 300 MW of electrolysers imposed

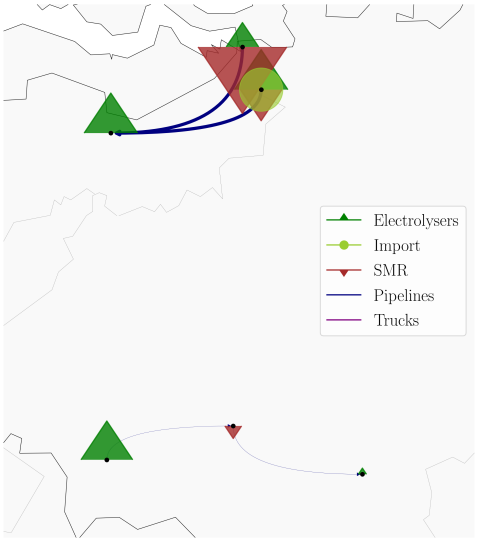

Figure 4.20: Optimal network minimizing the total cost, with 1GW of electrolysers imposed

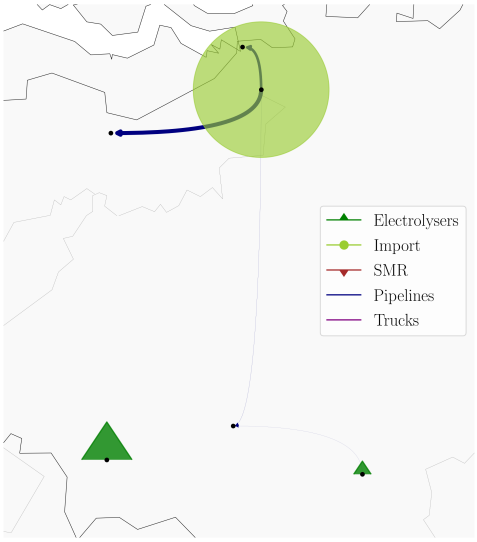

Figure 4.21: Optimal network minimizing the emissions, with 300 MW of electrolysers imposed

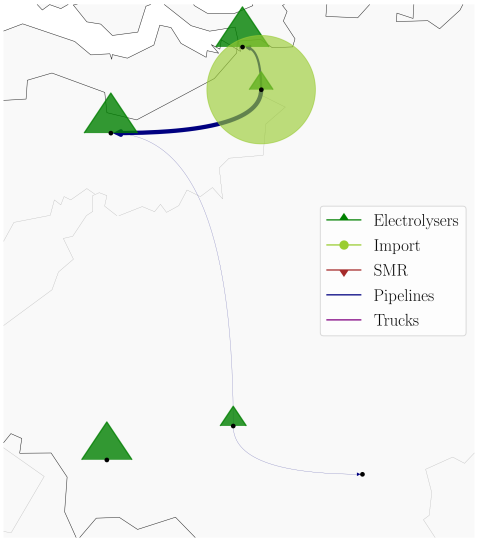

Figure 4.22: Optimal network minimizing the emissions, with 1 GW of electrolysers imposed

In Figure 4.24, the breakdown of the costs for 1000 MW of electrolysers imposed. It confirms that the price of electricity is the main obstacle against viability of electrolysers,

since the annualized Capex of electrolysers represents a negligible fraction of the total cost.

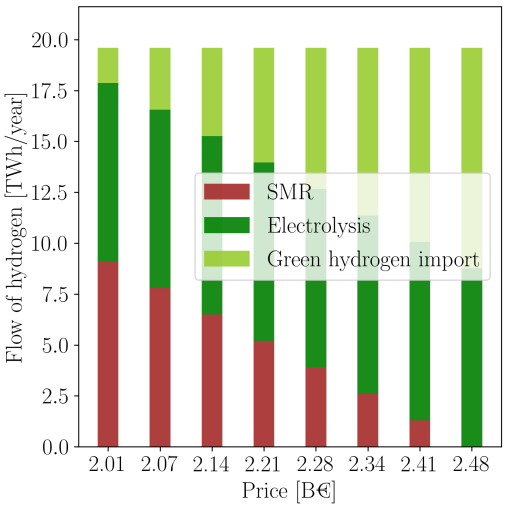

Figure 4.23: Mix of hydrogen produced/imported through the Pareto front, with 1 GW of electrolysers imposed

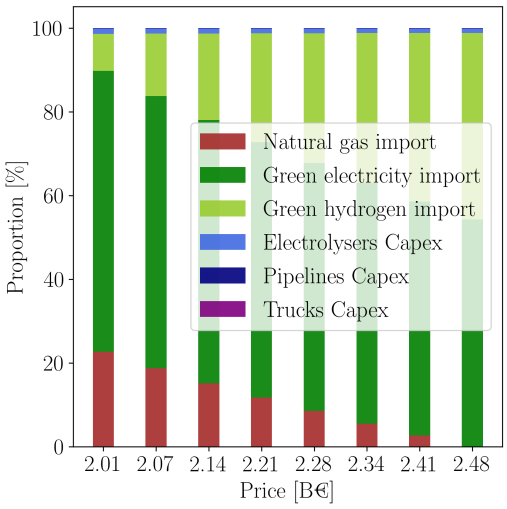

Figure 4.24: Breakdown of total cost through the Pareto front, with 1 GW of electrolysers imposed

4.2.3 Influence of resources prices

In the last section, the impact caused by imposing a given total capacity of electrolysers in Belgium was discussed. However, it was based a series of assumptions on the input data (demand, prices, ...). Then, the additional cost computed was relevant only compared to the reference scenario. In practice, there are a lot of uncertainties concerning the assumptions taken. It is especially true concerning the evolution of the prices for the resources. If electrolysis is not profitable in the reference scenario, it could be in other scenarios, if variations of the resource prices are envisaged for example.

Natural gas

Huge uncertainties concern the evolution of the natural gas market. It is even more evident following the geopolitical situation between Europe and Russia with the war in Ukraine. Some of the European countries have today the public intention to diversify their supply and to reach an energy independance from Russia. For example, Germany, the largest European importer, intends to be able to enforce a Russian oil ban by the end of 2022 [50]. It is however not a common position within the European Union, since all countries have to ensure their energetic safety and the Russian dependency strongly varies from one country to another. Even more important, we clearly lack of perspective about these recent events and the consequences in the future years. That is why we will

use in this section only predictions anterior to the Ukrainian war.

For the reference scenario, an average predicted price for natural gas for the period of 2030 was adopted. In all the scenarios, the prices are expected to grow, with more or less intensity. The trend will continue until 2050. From the same source [44], we can extract the predicted prices for 2050, similarly to what was done in Table 4.7. With this set of data, for the two periods of time, we can extract more pessimistic scenarios for the price of natural gas. We can compute the different quartiles among all the scenarios, and we choose to compare the reference solution with cases where the price of natural gas increases up to 48€/MWh and 63€/MWh, corresponding respectively to the third quartile and the maximal value.

	Price [€/MWh]
Min	19
25	35
50	40
75	48
Max	63

Table 4.11: Scenarios for price of natural gas for the horizon 2030-2050

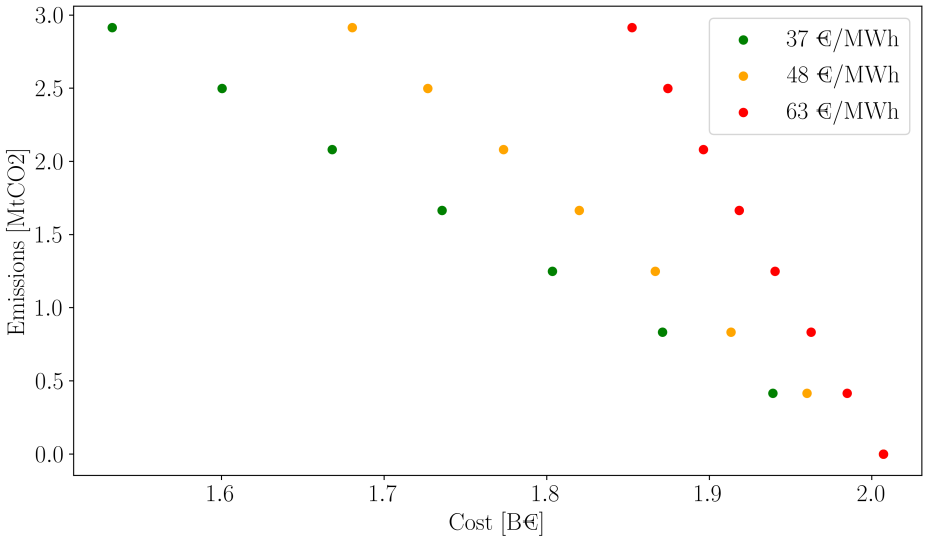

Figure 4.25: Pareto fronts with different prices of natural gas (average, 3rd quartile and maximum)

In Figure 4.25, the Pareto fronts for the different scenarios are represented. If the price of natural gas increases, then the difference in cost between the two extreme solutions of the Pareto front is reduced. Compared to the reference case, where 30% of

cost augmentation are required to reach zero emissions, it could be lowered to 19% or 8% respectively. Indeed, the optimum associated to minimal emissions is not impacted by the price of natural gas, since it is based on a 100% import of hydrogen, with no SMRs remaining operational. On the contrary, the optimum associated to minimal total cost is in majority dependent on the gas market. We can note that using natural gas in existing SMRs would probably stay the most economic option compared to imported hydrogen or local electrolysis.

Hydrogen and electricity

Concerning the prices of hydrogen and electricity, in theory we can not state that they are totally uncorrelated. There is not a direct link between the two parameters, but for example, if the levelized cost of energy (LCOE) for renewables drops, there will be an impact on the price of both imported hydrogen and imported green electricity. However, there is no way to measure this respective impact. Moreover, the markets in Europe and the rest of the world can be very different from one to another, at the level of taxes, subsidies, ... That is why we adopt the assumption of uncorrelated prices.

In the reference scenario, imported hydrogen is clearly the most competitive option. In this section, we will try to find in which conditions the energy market should move to make the installation of onsite small units of electrolysers an economically viable option. To do so, a sensitivity analysis is conducted, with the prices of hydrogen and electricity varying between extreme values, corresponding to the best- and the worst-case scenarios.

The main obstacle against the viability of electrolysers is the high price of electricity. From the source [40] where was extracted the average price of imported hydrogen, the average price for producing electricity is of around 45€/MWh. It is in a completely different range from average price in European Union considered in the reference scenario, of 100€/MWh. It is due to multiple factors:

- One crucial assumption is on the prices of green electricity for the retail market. It means that, between the producer and the consumer (here the potential Belgian industries building electrolysers), there is a third actor: the reseller. The reseller can be electricity utility companies, electricity marketers, ... The prices excluding the reseller margin are included in what is called "wholesale market". If we take a look at the evolution of the gross prices of electricity in Europe, the prices oscillate around 40 €/MWh in 2017, which is closer to the price of 45 €/MWh cited before. Indeed, for the case of imported hydrogen, it is probably produced more locally, closer to the source of electricity. The producer of electricity could be the same producer of hydrogen, lowering the costs of electricity. It is absolutely not the case for Belgium, where green electricity must be imported from abroad, for higher prices.

- Countries like Australia, Chile or Oman, have a very large green potential for renewables. For example, the potential capacity factor for solar panels in Chile is

in average larger than 0.3, around 2 times superior than neighboring countries as Netherlands or Germany [51][52]. It allows the construction of very high capacities for renewables, with high productivity. In large majority, electricity produced in large quantity minimizes the costs of production.

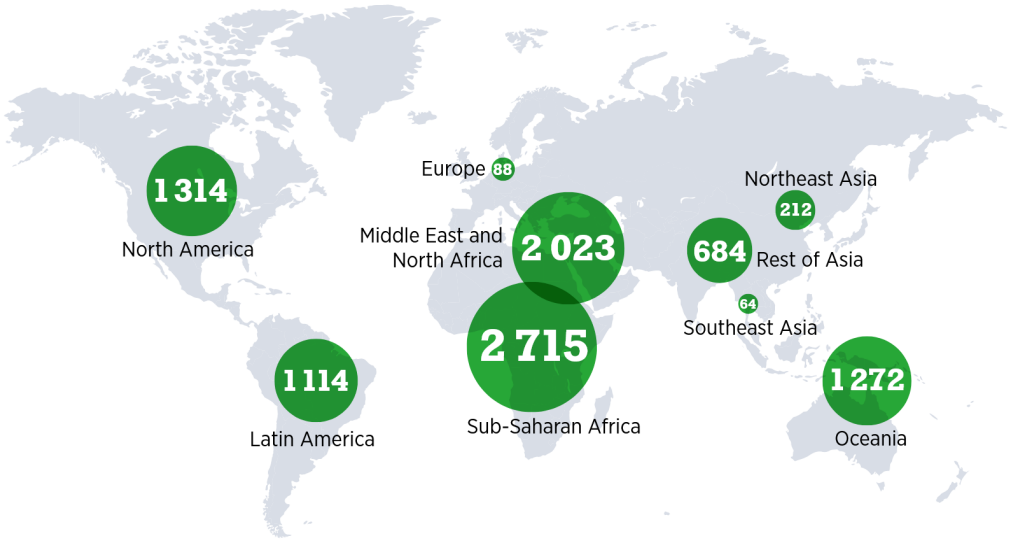

Figure 4.26: Technical potential for producing green hydrogen under USD 1.5/kg by 2050, in EJ [53]

If we compare in Figure 4.26 the technical potential to produce green hydrogen at low price by 2050, it is clear that Europe a negligible actor in the global market, far from Africa, South and North America and Oceania.

- Electricity transported by cable can be up to 20 times more expensive than hydrogen [48], making the transport of hydrogen very competitive.

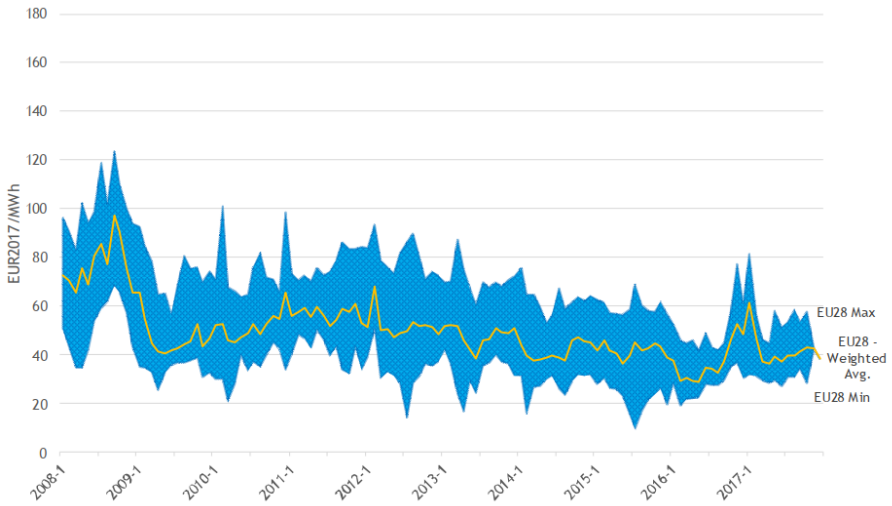

Figure 4.27: Wholesale electricity prices in Europe from 2008 to 2017 [54]

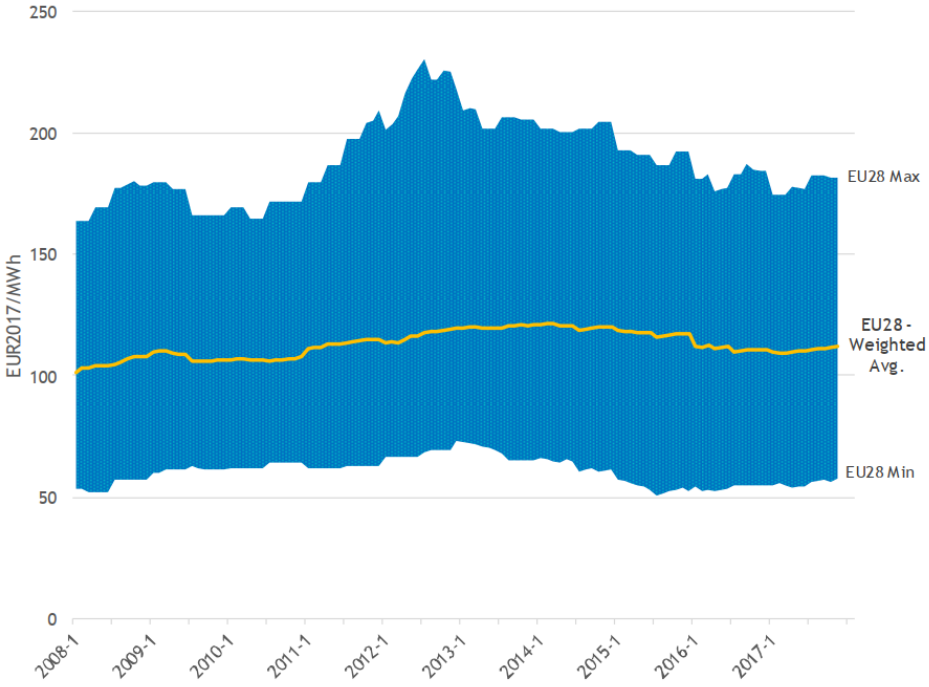

Figure 4.28: Electricity prices for industrial retail in Europe from 2008 to 2017 [54]

The price of electricity could also stay at a higher level. For the sensitivity analysis, we consider that the price of electricity oscillates between 40 and 110 €/MWh.

Huge uncertainties are also related to the import of hydrogen from abroad. The value of 102 €/MWh was an average value, but worst and best cases can also be extracted from [40]. We consider that in best case, the price of imported hydrogen would be of 90 €/MWh, and in worst case of 125 €/MWh.

For the sensitivity analysis, a resolution of 5€/MWh is adopted. For the considered range of prices, it means that $8 \cdot 16 = 120$ unique combinations for price of hydrogen and electricity exist. 120 independent runs are conducted, and for each run, the presence of electrolysers is evaluated at the extreme point of Pareto set, corresponding to optimum in terms of emissions. In Figure 4.29 the total capacity of electrolyser (MW) in each run for the zero emissions case is represented. The total capacity oscillates between 0 MW, where no electrolyser is installed, due to a non-competitiveness of electricity, and 1800 MW, where the maximal capacity (300MW) is installed on each of the 6 nodes. It can be observed that, depending on the price of imported hydrogen, the price of electricity should fall under 80 €/MWh or 60 €/MWh to have an installation of electrolysers. In the case of the reference scenario, where the price of hydrogen was around 100 €/MWh, the price of electricity should have been under 65 €/MWh. At 100 €/MWh, it was far from the transition region.

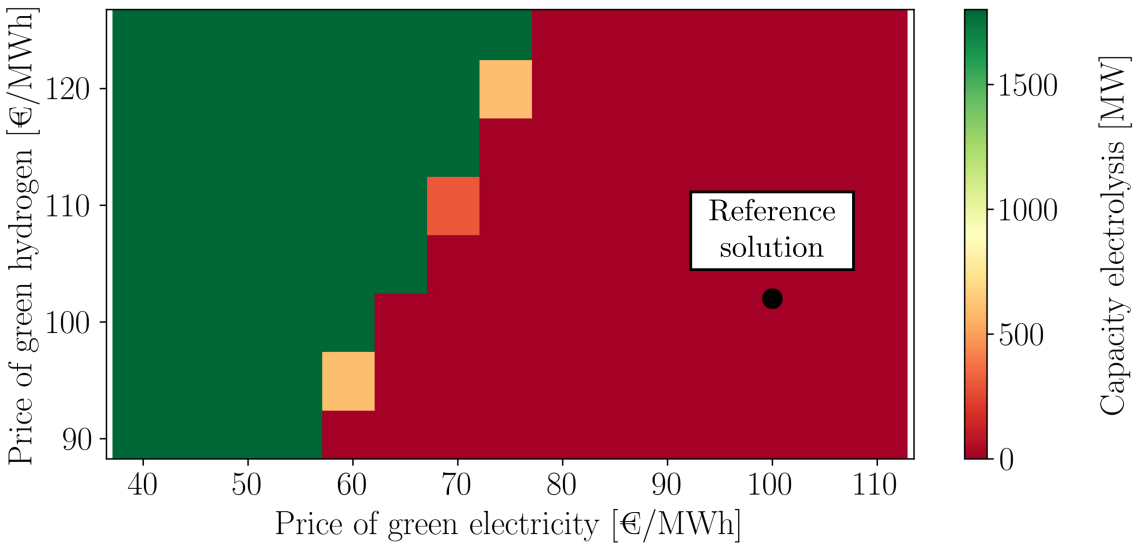

Figure 4.29: Sensitivity analysis. It shows the capacity of electrolysis installed for the zero emissions optimum, depending on the prices of imported green hydrogen and imported green electricity.

Regarding the evolution of the total cost between the two extreme cases (minimum price for both electricity and hydrogen and the situation with the maximum), there is an increase from 1.36 billion € to 2.46 billion €, representing an increase of 80%. It is an important difference, and it illustrates that the evolution of the market has a strong influence on the total costs. The variation of the costs is represented in Figure 4.30, again for the optimum in terms of emissions.

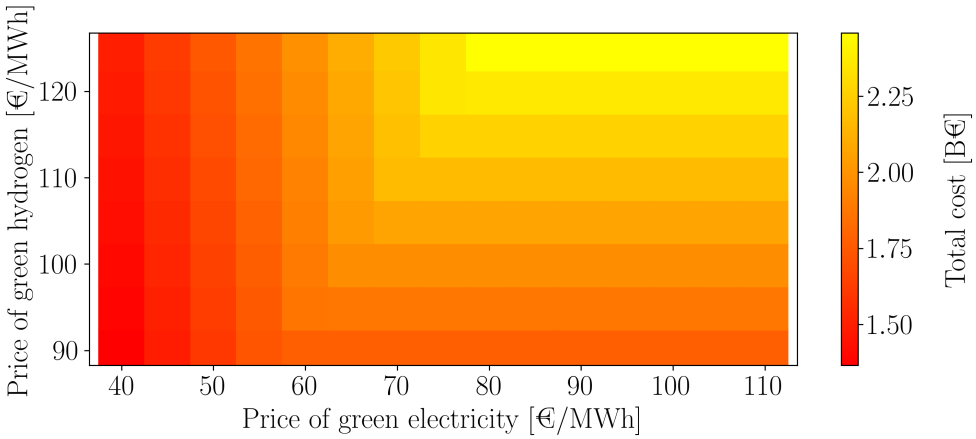

Figure 4.30: Total cost in the sensitivity analysis. It shows the total cost for the zero emissions optimum, depending on the prices of imported green hydrogen and imported green electricity.

Finally, the resolution of the sensitivity analysis is augmented around the transition region, and the result is shown in Figure 4.31. Here is the confirmation that there is a progressive switch between zero and full installation of electrolysers all along the transition region.

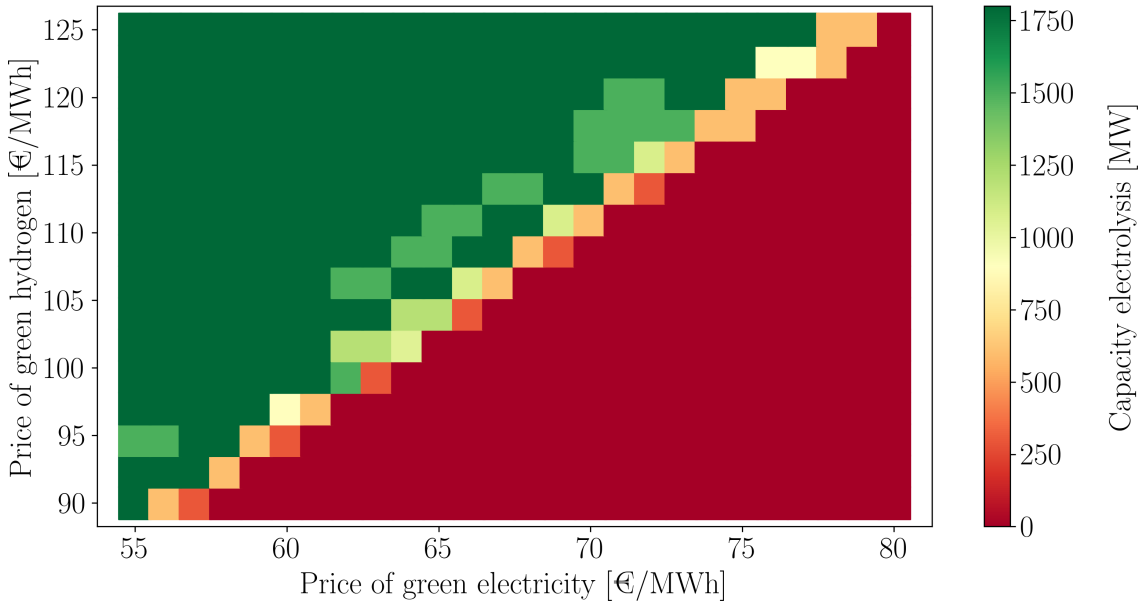

Figure 4.31: Refined sensitivity analysis. It shows the capacity of electrolysis installed for the zero emissions optimum, depending on the prices of imported green hydrogen and imported green electricity, with higher resolution around transition region.

Chapter 5

Conclusion and perspectives

Through this master thesis, a hybrid metaheuristic algorithm was sucessfully adapted for multi-objective optimization, able to deal with complex Hydrogen Supply Chain Design Network (HSCDN) problems. Applied to the case study of Belgium, the hybrid version offered similar performances compared to the simplified implementation.

The results concerning the case study of Belgium show a progressive switch from existing SMRs to imported green hydrogen, neglecting the development of local electrolysis. It is due to a high competitiveness of imported hydrogen compared to the market of electricity in Europe. In these conditions, decreasing the CO_2 emissions from actual 2.9 Mt to zero would cause an increase of the costs of 30% compared to the optimum in term of costs.

Installing electrolysis in Belgium is not optimal from financial considerations. If we do want to impose a total of 1 GW of electrolysers, it would cause a cost increase of 27% compared to the optimal solution. Depending on the assumptions made about the prices of imported green hydrogen, the price of electricity should fall between 60€/MWh and 80€/MWh to make electrolysis profitable, compared to the price of 100€/MWh considered in reference case.

Yet, the use of metaheuristic is not justified for this case study. It implies a higher computational cost while offering similar performances compared to the simplified version. It allows to validate the implementation, but adding other sources of non-linearities is mandatory in order to justify the use of the hybrid metaheuristic. For example, the pressure levels between the nodes could be introduced in the model, because the equations characterizing the pressure drops and the compressions are very difficult to linearize.

Moreover, the developed tool can be applied to less trivial cases than Belgium. For example, an analysis could be conducted on larger countries with more dense nodal representation, as France or Germany. It could also be used to analyze the optimal HSCND at a higher level, for example at the level of the European Union. It would allow to provide a coherent strategy between the whole set of states and see the interconnections. Other technologies can also be introduced, as SMRs coupled with Carbon Capture and Storage

(CCS) providing "blue" hydrogen, which is neglected in this simple analysis.

Another weakness of this implementation is the lack of robustness. All the parameters are fixed and the design returned by the algorithm is optimal only for the scenario considered. As demonstrated, variations in the prices of resources are propagated to the total cost. However, many uncertainties rely on the hydrogen market. A stochastic modeling would be a valuable asset in a future version of the tool, allowing to manage uncertainties in the estimated costs or demand and improving the robustness of the design against deviations from the expected scenario.

Finally, as the model used is very generic, it could be used in other applications than strict hydrogen production. For example, the further transformation of hydrogen into synthetic fuels could be studied with the tool, or even the management of CO_2 after capture if CCS are considered.

Appendix A

Various implementations of ACO

A.1 Ant Colony System

Adapted State Transition Rule

When different paths have very close lengths, the simple state transition rule can be too slow to converge. The differences between paths are not important enough for the algorithm to be effective. The solution is to adapt the state transition rule, to make it more sensitive to the best paths.

What the authors proposed in the paper [13], is to use the classical probability for moving between the nodes only in a certain proportion; the rest of the time, the ant will choose simply the best path leaving the node where it stayed. This proportion is regulated via a simple random choice, for example between [0,1], and if the number picked is higher than a certain parameter q_0, the best path is followed, otherwise the classical state transition rule S is applied. This allows to have a better repartition between exploration and exploitation.

$$s = \begin{cases} \arg\max_{u \in J_k(r)} \left\{ [\tau(r,u)] \cdot [\eta(r,u)]^{\beta} \right\} \text{ if } q \leq q_0 \quad \text{(exploitation)} \\ S, \text{ if } q < q_0 \text{ (biased exploration)} \end{cases} \tag{A.1}$$

Global pheromone Updating

The original updating rule, performed at the end of each iteration, allowed all the ants to deposit pheromone on their paths, the quantity $\Delta\tau(r,s)$ depending on the quality of their path. In the reference paper, they chose, for enhancing best solutions, to only allow the best ant to drop pheromone; the others won't have any contribution. Two options

are possible: either the "global best path" is reinforced, either the "iteration best path". The two have similar performances.

$$\tau(r,s) \leftarrow (1-\rho)\cdot\tau(r,s) + \cdot\Delta\tau(r,s) \tag{A.2}$$

where

$$\Delta\tau(r,s) = \begin{cases} (L_{gb})^{-1}, & \text{if } (r,s) \in \text{ global-best-tour} \\ 0, & \text{otherwise} \end{cases}$$

$0 < \alpha < 1$ is the pheromone decay parameter, and L_{gb} is the length of the globally best tour from the beginning of the trial.

Local pheromone Updating

Finally, another addition is to allow the ants to change dynamically during their travel the quantity of pheromone $\tau(r)$. This allows to change the attraction of edges dynamically, by decreasing slightly the level of pheromone after an ant passes on it. It means that it allows the ants to try other paths than the best found, and to increase the exploration. As exploitation is mainly developed in the two first improvements, the local updating rule is the counter-weigth, favoring exploration instead.

$$\tau(r,s) \leftarrow (1-\alpha)\cdot\tau(r,s) + \alpha\cdot\Delta\tau(r,s) \tag{A.3}$$

The expression chosen by the authors for the increment of pheromone $\Delta\tau(r)$ is τ_0, the initial level of pheromone. The initial level of pheromone is roughly estimated via a pure heuristic evaluation of the optimal cost.

A.2 Min Max formulation

This version, one of the most popular among ACO, has two special purposes: first, again, give more weight to the best solutions found, and second, limit the impact of the search stagnation.

Global pheromone updating

In this formulation, only one single ant is authorized to drop pheromone after each iteration, as in the ACS formulation. The pheromone update is given by the modified expression:

$$\tau(r,s) \leftarrow (1-\rho)\cdot\tau(r,s) + \cdot\Delta\tau(r,s), \tag{A.4}$$

where:

$$\Delta\tau(r,s) = \begin{cases} (L_{ib})^{-1}, & \text{if } (r,s) \in \text{ iteration-best-tour} \\ 0, & \text{otherwise.} \end{cases}$$

$0 < \rho < 1$ is the pheromone decay parameter, and L_{ib} is the length of the best tour during the current iteration. In the paper [55], the choice between global and iteration-best-tour is discussed. The application of the global best during the first iterations forces the algorithm to converge faster, but the exploration is reduced. A more complex option is to implement a dynamic switch between global and iteration best, to get adaptability to the current iteration, but in this document iteration-best-tour is chosen.

Pheromone limit

Search stagnation occurs when all the ants follow the same path again and again, such that better solutions cannot be found anymore. What happens is that, for each node, among all the possible arcs leaving this node, one has a much larger amount of pheromone on it. Then the ants will go preferably through this arc. This issue can appear for example when the algorithm is stuck in a local minimum.

What is proposed in this version is to impose a maximal level of the pheromone, to avoid a too high level of pheromone on some trails. A lower bound is also imposed. The expressions given in [55] are the following:

$$\tau_{\max} = \frac{1}{1-\rho}\frac{1}{f\left(s^{\text{opt}}\right)}, \tag{A.5}$$

$$\tau_{\min} = \frac{\tau_{\max}\left(1 - \sqrt[n]{p_{\text{best}}}\right)}{(\text{avg} - 1)\sqrt[n]{p_{\text{best}}}}. \tag{A.6}$$

These levels of pheromone can evolve dynamically, with dynamic evaluation of optimal cost. Convergence is reached when the maximal and minimal levels are stabilized.

A.3 Elitist formulation

This version is closer to AS, and introduces two types of ants: the classic and the elitist ones. The elitist ants are able to cooperate directly with the rest of the colony; they are aware of the best path found from the first iteration, and are able to drop pheromone on it. The normal ants are behaving normally like in AS.

The combination between the two leads to a better enhancing of the best solutions, but the proportion of elitist ants must be chosen carefully ; if there are too many, the level of exploration will be too low to reach optimal solutions.

A.4 Comparative study

To compare the four different implementations, several parameters were chosen to be common between the versions. By default, we set: $\alpha = 1$, $\beta = 5$, number of ants $= 25$, $\rho = 0.8$. The maximal number of iterations is fixed at 1000. It means that the maximal number of function evaluations, computed as the number of ants $\times$ number of iterations, is set at 25000. The criteria of convergence is: stop the algorithm if, during f trials (f is chosen as the number of ants), the difference between previous and current optimal solution is lower than ϵ, here equal to 0.001. It is then an absolute criteria of convergence. This criteria helps to avoid a too early convergence: often a few iterations are necessary to explore around a local minimum to find a lower one.

The comparison is made on 3 different problems, with respectively 25, 50, and 100 nodes, all having xy coordinates between 0 and 1. The coordinates of the problems are generated randomly. For each problem, each of the 4 algorithms runs for 25 independent trials.

In figures A.1,A.2 and A.3, for each problem, the distribution of optimal solutions found during the 25 trials is presented, for the four different implementations. The results are organized under the form of "boxplot", showing the locality, spread and skewness groups of numerical data through their quartiles [61]. We can observe that, as a general trend, with the complexity increasing with the number of nodes, the number of successful trials (the trials where the global optimal solution is found) decreases, and some versions are even far from reaching this optimum. The classical AS becomes less and less efficient with increasing the number of nodes, and the differences with other formulations becomes more visible. ACS and Min-Max formulation present better results: ACS finds for each case the best solution, but presents a less good distribution than the Min-Max formulation. There is an exception for the 50 nodes problem, where the Min-Max presents a very poor distribution even if outliers are very close to the optimum. An advanced study should be required to explain this irregularity.

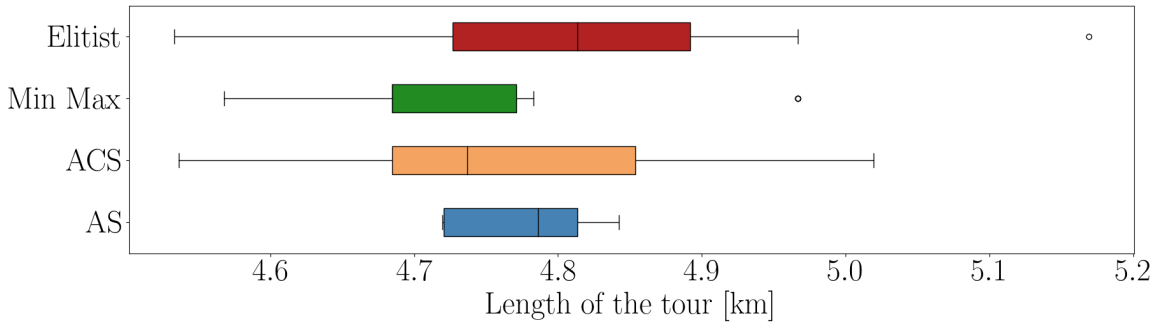

Figure A.1: Results for 25 nodes problem

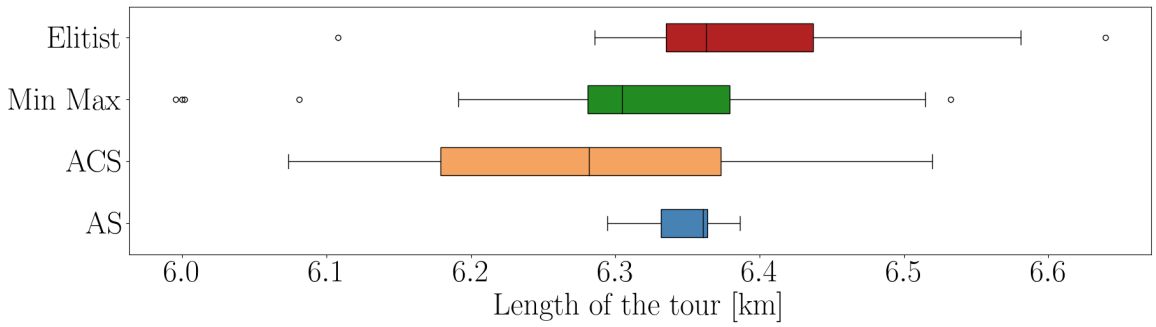

Figure A.2: Results for 50 nodes problem

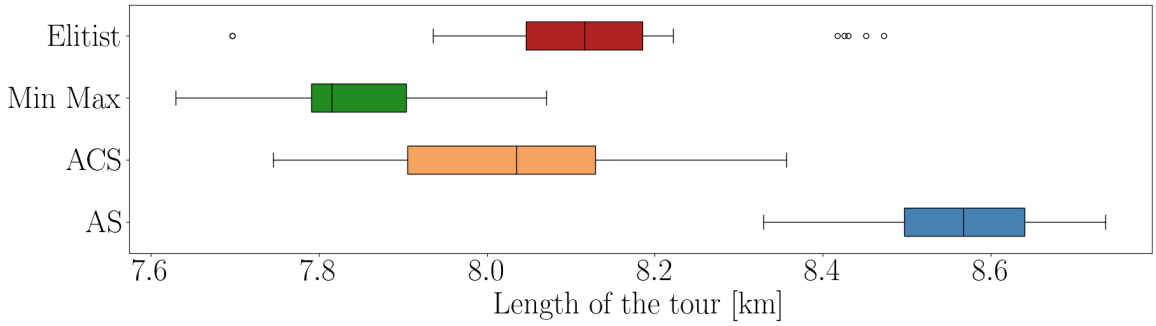

Figure A.3: Results for 100 nodes problem

The table A.1 presents the results above: average best tour's length found, best tour's length found and standard deviation of the sample. In addition, it shows the average number of Function Evaluations (FEs) in each case; it is given by number of ants $\times$ number of iterations for each run. The boxes shaded in green represent the best value for each problem among the 4 implementations.

In general, we can state that the Min-Max formulation has the best average solution, and except for 25 nodes, it also offers the best solution. In a second place, ACS offers comparable performances. However, there seems to be a trade-off between speed of convergence and quality of the solutions. Even if the Min-Max presents better average values than the ACS, it requires an higher number of FEs.

The AS, compared to the other implementations, is not able to find the best value, but also has a lower standard deviation in general: this denotes the lack of exploration described earlier. Elitist formulation offers very disappointing performances, and requires probably a finer tuning of the parameters.

	AS				**ACS**			
	average	std dev	best	FEs	average	std dev	best	FEs
25 nodes	4,77	0,04	4,72	1040	4,76	0,13	4,54	1038
50 nodes	6,35	0,02	6,29	1318	6,29	0,13	6,07	1345
100 nodes	8,56	0,11	8,33	1232	8,03	0,16	7,75	1960
	Min-Max				**Elitist**			
	average	std dev	best	FEs	average	std dev	best	FEs
25 nodes	4,72	0,11	4,57	1415	4,80	0,13	4,53	1124
50 nodes	6,29	0,14	6,00	1699	6,40	0,11	6,11	1449
100 nodes	7,85	0,10	7,63	3289	8,13	0,20	7,70	1800

Table A.1: Results for 25,50 and 100 nodes for the 4 methods

Finally, here under on A.5, A.7 and A.9, a graphical representation of the best path found among the 4 implementations is shown. For the problems of 25 and 50 nodes, it has the appearance of a real optimal solution, but for 100 nodes, a better path seems to exist. To ensure that this solution is not optimal, an exact method should be required. However, the associated computational cost does not seem realistic. To solve traveling salesman problem with "brute-force" method, the algorithm should compute all possible roads, and then pick the shortest one. This approach would result in a complexity of $\Theta(n!)$: for 100 nodes, the complexity would be around 10^{157}, which is hardly solvable. Other alternative exist, as Held–Karp algorithm, a well known dynamic programming algorithm, having a complexity of $\Theta(2^n n^2)$ [7]. It would reduce the complexity to 10^{33}, far from a brute force algorithm, but yet very important, justifying the use of metaheuristics.

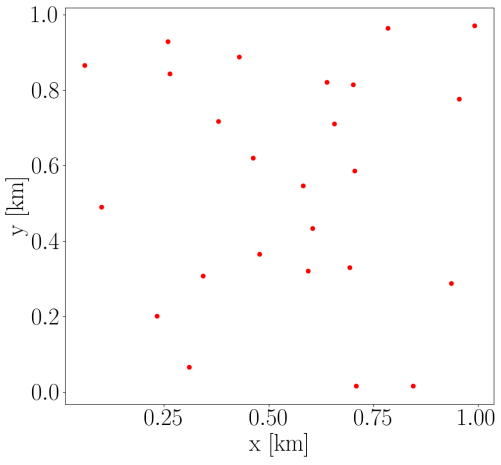

Figure A.4: TSP: 25 nodes

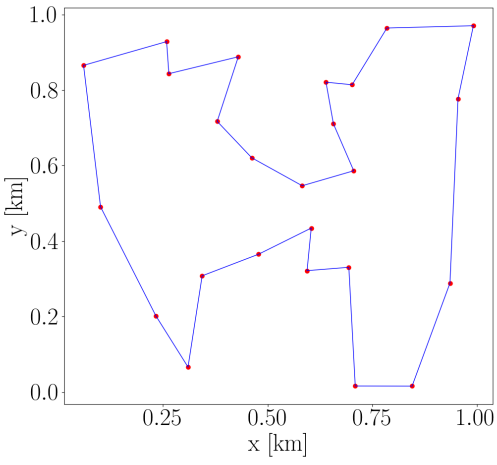

Figure A.5: Best path found (25 nodes)

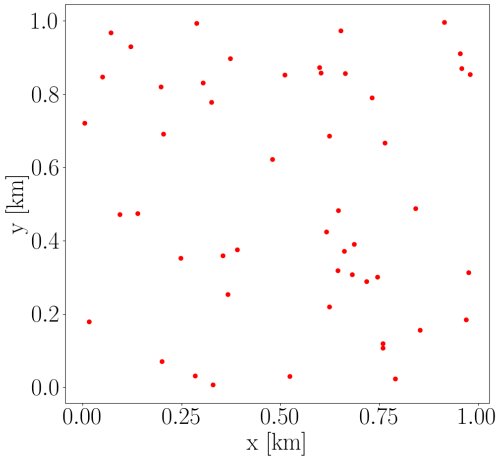

Figure A.6: TSP: 50 nodes

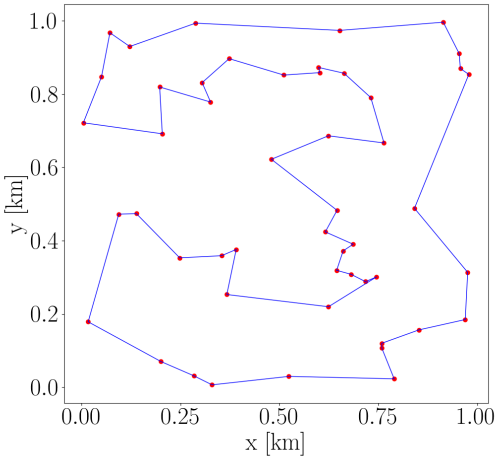

Figure A.7: Best path found (50 nodes)

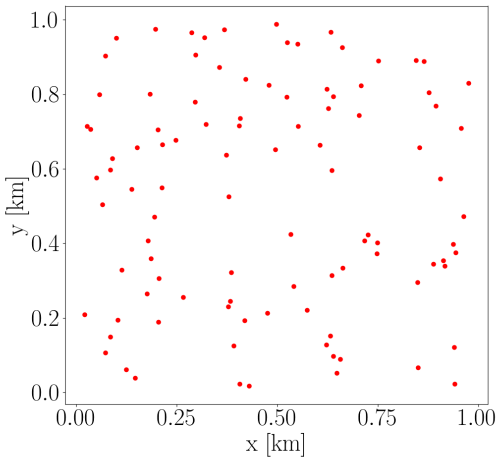

Figure A.8: TSP: 100 nodes

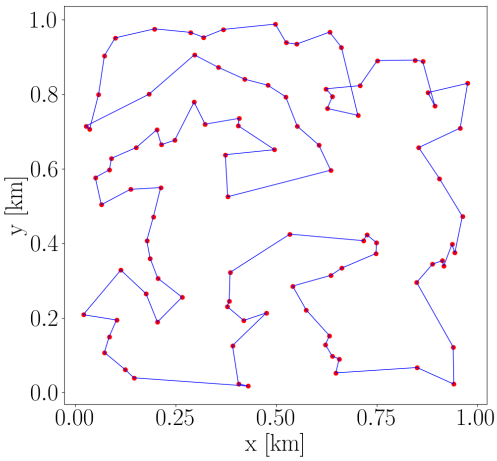

Figure A.9: Best path found (100 nodes)

Appendix B

Notation, inputs and outputs of the optimization model

Table B.1: Sets used in the model formulation.

Sets	Description
$\mathcal{C}$	carriers (*setCarriers*)
$\mathcal{H}$	conversion technologies (*setConversionTechnologies*)
$\mathcal{K}$	transport technologies (*setTransportTechnologies*)
$\overline{\mathcal{L}}$	import carriers over the system boundaries (*setImportCarriers*)
$\underline{\mathcal{L}}$	export carriers over the system boundaries (*setExportCarriers*)
$\mathcal{N}$	nodes (*setNodes*)
$\mathcal{T}$	time steps (*setTimeSteps*)
$\mathcal{S}$	scenarios

Table B.2: Auxiliary sets used in the model formulation. The parenthesis indicates a dependency of the elements of the set from the elements of another set.

Sets	Description
$\mathcal{D}((\mathcal{H}\|\mathcal{K}),\mathcal{N})$	combination of technologies with nodes for conversion technologies and pairs of nodes (edges) for transport technologies (*setTechnologyLocation*)
$\overline{\mathcal{F}}(\mathcal{H},\overline{\mathcal{J}}(\mathcal{H}))$	combination of technologies with the respective input carriers (*setInputCarriersTechs*)
$\underline{\mathcal{F}}(\mathcal{H},\underline{\mathcal{J}}(\mathcal{H}))$	combination of technologies with the respective output carriers (*setOutputCarriersTechs*)
$\mathcal{G}(\mathcal{K},\mathcal{Q}(\mathcal{K}))$	combination of technologies with the respective carriers (*setTransportCarriersTech*)

$\overline{\mathcal{J}}(\mathcal{H})$	input carriers of conversion and transport technologies (*setInputCarriers*)
$\underline{\mathcal{J}}(\mathcal{H})$	output carriers of conversion and transport technologies (*setOutputCarriers*)
$\mathcal{Q}(\mathcal{K})$	transport carriers of transport technologies (*setTransportCarriers*)
$\mathcal{P}(\mathcal{H})$	dependent carriers of conversion and transport technology (setDependentCarriers)
$\mathcal{R}(\mathcal{H}\|\mathcal{K})$	reference carriers of conversion and transport technology (*setReferenceCarriers*)

Table B.3: Input parameters to the optimization model.

Parameter	**Description**	**Domain**	**U.m.**
$d_{j,i}$	demand of carrier j at node i (*demandCarrier*)	$\mathbb{R}_+$	MWh
$u_{j,i}$	import price of carrier j at node i (*importPriceCarrier*)	$\mathbb{R}_+$	EUR/MWh
$v_{j,i}$	export price of carrier j at node i (*exportPriceCarrier*)	$\mathbb{R}_+$	EUR/MWh
$a_{j,i}$	availability of carrier j at node i (*availabilityCarrier*)	$\mathbb{R}_+$	MWh
$p_h^{\min}$	minimum load of conversion technology h (*minLoadConversionTechnology*)	$\mathbb{R}_+ \cap [0,1]$	-
$p_k^{\min}$	minimum load of transport technology k (*minFlow*)	$\mathbb{R}_+ \cap [0,1]$	-
$s_{h,i}^{\max}$	maximum capacity of conversion technology h in node i (*maxPotentialCapacity*)	$\mathbb{R}_+$	MW
$s_{k,i}^{\max}$	maximum allowed capacity of transport technology k in node i (*maxPotentialCapacity*)	$\mathbb{R}_+$	MW
$\Delta s_h^{\min}$, $\Delta s_h^{\max}$	minimum and maximum capacity allowed capacity expansion of conversion technology h	$\mathbb{R}_+$	MW
$\Delta s_k^{\min}$, $\Delta s_k^{\max}$	minimum and maximum capacity allowed capacity expansion of transport technology k	$\mathbb{R}_+$	MW
$l_{k,i,i'}$	distance between nodes i and i' for transport technology k (*distance*)	$\mathbb{R}_+$	km

$i_{k,i,i'}$	halved cost per unit distance of the non-directional capacity connecting nodes i and i' for transport technology k (*costPerDistance*)	$\mathbb{R}_+$	EUR/km
k_k	loss coefficient per unit of distance for transport technology k (*lossFlow*)	$\mathbb{R}_+$	1/km
t^l_h	lifetime of conversion technology h (*lifetimeConversionTechnology*)	$\mathbb{N}$	
t^l_k	lifetime of transport technology k (*lifetimeTransportTechnology*)	$\mathbb{N}$	
t^e_h	expansion time required for conversion technology h	$\mathbb{N}$	
t^e_k	expansion time required for transport technology k	$\mathbb{N}$	

Table B.4: Decision variables (DV) returned by the optimization model.

Variable	**Description**	**Domain**	**U.m.**
$y_{h,i}$	scheduling of operation of conversion technology h at node i (*selectConversionTechnology*)	{0,1}	-
$z_{h,i}$	expanding the capacity of conversion technology h at node i, subject to installation time t^i_h (*expandConversionTechnology*)	{0,1}	-
$y_{k,i,i'}$	scheduling of operation for transport technology k from node i to node i' at under scenario s (*selectTransportTechnology*)	{0,1}	-
$z_{k,i,i'}$	expanding the capacity of transport technology k from node i to node i' at under scenario s (*expandTransportTechnology*)	{0,1}	-
$S_{h,i}$	capacity of conversion technology h at node i (*capacity*)	$\mathbb{R}_+$	MW
$S_{k,i,i'}$	capacity of transport technology k from node i to node i' at under scenario s (*capacity*)	$\mathbb{R}_+$	MW
$dS_{h,i}$	capacity increase of conversion technology h at node i (*builtCapacity*)	$\mathbb{R}_+$	MW
$dS_{k,i,i'}$	capacity increase of transport technology k from node i to node i' at under scenario s (*builtCapacity*)	$\mathbb{R}_+$	MW

$G_{j,h,i}$	input stream of carrier j into conversion technology h at node i (*inputFlow*)	$\mathbb{R}_+$	MWh/y
$P_{j,h,i}$	output stream of carrier j from conversion technology h at node i (*outputFlow*)	$\mathbb{R}_+$	MWh/y
$F_{j,k,i,i'}$	flow of carrier j through transport technology k from node i to node i' (*carrierFlow*)	$\mathbb{R}_+$	MWh/y
$U_{j,i}$	import of carrier j into node i from the grid under scenario s (*importCarrierFlow*)	$\mathbb{R}_+$	MWh/y
$V_{j,i}$	export of carrier j from node i to the grid under scenario s (*exportCarrierFlow*)	$\mathbb{R}_+$	MWh/y

Table B.5: Input functions to the optimization model.

Function	**Input**	**Description**	**Codomain**	**U.m.**
c_h	$S_{h,i}$	function mapping the size of the conversion technology h to its installation cost under scenario s (*capex*)	$\mathbb{R}_+$	EUR
o_h	$P_{h,i}$	function mapping the output stream of the conversion technology h to its operational cost under scenario s	$\mathbb{R}_+$	EUR
c_k	$C_{k,i,i'}$, $l_{k,i,i'}$	function mapping the size and the distance between nodes of the transport technology k to its installation cost under scenario s (*capex*)	$\mathbb{R}_+$	EUR
o_k	$F_{j,k,i,i'}$	function mapping the flow of the transport technology k to its operational cost under scenario s	$\mathbb{R}_+$	EUR
e_h	$S_{h,i}$	function mapping the size of the conversion technology h to its installation emissions under scenario s	$\mathbb{R}_+$	$\mathrm{t_{CO_2}}$
g_h	$P_{h,i}$	function mapping the output stream of the conversion technology h to its operational emissions under scenario s	$\mathbb{R}_+$	$\mathrm{t_{CO_2}}$
e_k	$C_{k,i,i'}$, $l_{k,i,i'}$	function mapping the size and the distance between nodes of the transport technology k to its installation emissions under scenario s	$\mathbb{R}_+$	$\mathrm{t_{CO_2}}$
g_k	$F_{k,i,i'}$	function mapping the flow of the transport technology k to its operational emissions under scenario s	$\mathbb{R}_+$	$\mathrm{t_{CO_2}}$
$\eta_{h,j,j'}$	$S_{h,i}$, $G_{j,h,i}$, $P_{j,h,i}$	function mapping the size, input and output stream of conversion technology h converting carrier j to carrier j'	$\mathbb{R} \cap [0,1]$	-
f_k	$F_{j,k,i,i'}$, $l_{k,i,i'}$	function mapping the flow and transport distance of carrier j with transport technology k between node i and i' to the transport losses (*carrierLoss*)	$\mathbb{R} \cap [0,1]$	-

Bibliography

[1] The European Commission. The european green deal, December 2019.

[2] United Nations. Paris agreement, 2015.

[3] The European Commission. A clean planet for all. a european strategic long-term vision for a prosperous, modern, competitive and climate neutral economy, November 2018.

[4] IRENA. *World Energy Transitions Outlook 2022: 1.5°C Pathway.* International Renewable Energy Agency, 2022.

[5] A. Wang, J. Jens, D. Mavins, M. Moultak, M. Schimmel, K. Leun, D. Peters, and M. Buseman. *EUROPEAN HYDROGEN BACKBONE : Analysing future demand, supply, and transport of hydrogen.* Guidehouse, June 2021.

[6] The European Commission. A hydrogen strategy for a climate-neutral europe, July 2020.

[7] Wikipedia. Held–karp algorithm. `https://en.wikipedia.org/wiki/Held%E2%80%93Karp_algorithm` accessed 2022-05-22.

[8] M. Dorigo, V. Maniezzo, and A. Colorni. Ant system: An autocatalytic optimizing process technical report 91-016. 02 1999.

[9] M. Dorigo, V. Maniezzo, and A. Colorni. Ant system: optimization by a colony of cooperating agents. 26(1):29–41.

[10] M. Dorigo and L.M. Gambardella. Ant colony system: a cooperative learning approach to the traveling salesman problem. 1(1):53–66.

[11] M. Dorigo, E. Bonabeau, and G. Theraulaz. Ant algorithms and stigmergy. 16(8):851–871.

[12] Wikipedia. Ant colony optimisation. `https://fr.wikipedia.org/wiki/Algorithme_de_colonies_de_fourmis` accessed 2021-09-25.

[13] M. Dorigo and L.M. Gambardella. Ant colony system: A cooperative learning approach to the traveling salesman problem. *IEEE TRANSACTIONS ON EVOLUTIONARY COMPUTATION*, 1:150 – 181, 1997.

[14] T. Liao, T. Stützle, M.A. Montes de Oca, and M. Dorigo. An unified ant colony optimization algorithm for continuous optimization. 234(3):597–609.

[15] T. Liao, K. Socha, M. A. Montes de Oca, T. Stutzle, and M. Dorigo. Ant colony optimization for mixed-variable optimization problems. 18(4):503–518.

[16] K. Miettinen. *Nonlinear Multiobjective Optimization*. International Series in Operations Research & Management Science. Springer US, 1999.

[17] G. Narzisi. Classic methods - for multi-objective optimization. page 36.

[18] D. Angus and C. Woodward. Multiple objective ant colony optimisation. 3(1):69–85.

[19] G. Leguizamón and C.A. Coello Coello. *Multi-Objective Ant Colony Optimization: A Taxonomy and Review of Approaches*, volume 78, pages 67–94. WORLD SCIENTIFIC.

[20] A. Garcia-Najera and J.A. Bullinaria. Extending ACOR to solve multi-objective problems.

[21] K. Deb, A. Pratap, S. Agarwal, and T. Meyarivan. A fast and elitist multiobjective genetic algorithm: NSGA-II. 6(2):182–197.

[22] D. Angus. Population-based ant colony optimisation for multi-objective function optimisation. In M. Randall, H.A. Abbass, and J. Wiles, editors, *Progress in Artificial Life*, volume 4828, pages 232–244. Springer Berlin Heidelberg. Series Title: Lecture Notes in Computer Science.

[23] T. Friedrich, P.S. Oliveto, D. Sudholt, and C. Witt. Analysis of diversity-preserving mechanisms for global exploration. 17(4):455–476.

[24] J. G. Falcón-Cardona and C.A. Coello Coello. A new indicator-based many-objective ant colony optimizer for continuous search spaces. 11(1):71–100.

[25] R.L. Becerra and C.A.C. Coello. Solving hard multiobjective optimization problems using ϵ-constraint with cultured differential evolution. In T.P. Runarsson, H-G. Beyer, E. Burke, J.J. Merelo-Guervós, L.D Whitley, and X. Yao, editors, *Parallel Problem Solving from Nature - PPSN IX*, volume 4193, pages 543–552. Springer Berlin Heidelberg. Series Title: Lecture Notes in Computer Science.

[26] J. Blank and K. Deb. pymoo: Multi-objective optimization in python. *IEEE Access*, 8:89497–89509, 2020.

[27] M.L. Bynum, G.A. Hackebeil, W.E. Hart, C.D. Laird, B.L. Nicholson, J.D. Siirola, J-P Watson, and D.L. Woodruff. *Pyomo–optimization modeling in python*, volume 67. Springer Science & Business Media, third edition, 2021.

[28] L. Bako and O. Yahya. Piecewise affine system identification: A least harmonic mean approach. In *2019 IEEE 58th Conference on Decision and Control (CDC)*, pages 2660–2665. IEEE.

[29] V.H. Cantú, C. Azzaro-Pantel, and A. Ponsich. A novel matheuristic based on bi-level optimization for the multi-objective design of hydrogen supply chains. 152:107370.

[30] G. Maisonnier, J. Perrin, R. Steinberger-Wilckens, and S.C. Trümper. "european hydrogen infrastructure atlas" and "industrial excess hydrogen analysis" PART II: Industrial surplus hydrogen and markets and production. page 86.

[31] P. Quaglia. Analysis of the hydrogen supply chain and optimization of a case study in italy. Master's thesis, Politecnico di Torino and EIfER, 2021.

[32] C. Kurrer. The potential of hydrogen for decarbonising steel production. page 8.

[33] Mitsubishi Heavy Industries. How hydrogen can decarbonize the steel industry and what it will take. `https://www.euractiv.com/section/energy-environment/infographic/how-hydrogen-can-decarbonize-the-steel-industry-and-what-it-will-take/` accessed 2022-04-01.

[34] C. Hoffmann, M. Van Hoey, and B. Zeume. *Decarbonization challenge for steel. Hydrogen as a solution in Europe*. McKinsey Company, October 2020.

[35] *European Steel in Figures*. EUROFER, 2021.

[36] A. Boulamanti and J.A. Moya. *Energy efficiency and GHG emissions: Prospective scenarios for the Chemical and Petrochemical Industry*. EUR 28471 EN.

[37] I. Dincer and C. Acar. Review and evaluation of hydrogen production methods for better sustainability. *International Journal of Hydrogen Energy*, 40(34):11094–11111, 2015.

[38] Wikipedia. Steam reforming. `https://en.wikipedia.org/wiki/Steam_reforming` accessed 2022-04-10.

[39] J.G. Speight. *Handbook of Industrial Hydrocarbon Processes*. Elsevier Science, 2010.

[40] Engie EXMAR Fluxys Port of Antwerp Port of Zeebrugge WaterofNet Flux50, DEME. Shipping sun and wind to belgium is key in climate neutral economy. hydrogen import coalition : Final report, January 2021.

[41] Wikipedia. Electrolysis. `https://en.wikipedia.org/wiki/Electrolysis` accessed 2022-04-21.

[42] G. Kakoulaki, I. Kougias, N. Taylor, F. Dolci, J. Moya, and A. Jäger-Waldau. Green hydrogen in europe – a regional assessment: Substituting existing production with electrolysis powered by renewables. 228:113649.

[43] European Commission. Directorate General for Energy., European Commission. Directorate General for Climate Action., and European Commission. Directorate General for Mobility and Transport. *EU reference scenario 2020: energy, transport and GHG emissions : trends to 2050.* Publications Office.

[44] N. Duić, N. Štefanić, Z. Lulić, G. Krajačić, T. Pukšec, and T. Novosel. *EU28 fuel prices for 2015, 2030 and 2050.* Heat Roadmap Europe, November 2017.

[45] J.K. Helgaker. Transportation of hydrogen gas in offshore pipelines: H2pipe. `https://www.dnv.com/article/transportation-of-hydrogen-gas-in-offshore-pipelines-h2pipe-213006` accessed 2022-04-5.

[46] A. Wang, P. Peters, K. Leun, and M. Buseman. *European Hydrogen Backbone : HOW A DEDICATED HYDROGEN INFRASTRUCTURE CAN BE CREATED.* July 2020.

[47] Office of Energy Efficiency and Renewable Energy. Gaseous hydrogen delivery. `https://www.energy.gov/eere/fuelcells/gaseous-hydrogen-delivery` accessed 2022-04-23.

[48] European Energy Forum. *Discovering the molecule of the future: Session 1: Hydrogen from production to distribution and storage.* October 2020.

[49] P. Gabrielli, M. Gazzani, E. Martelli, and M. Mazzotti. Optimal design of multi-energy systems with seasonal storage. 219:408–424.

[50] M. (BBC) Race. Eu divided over how to step away from russian energy. `https://www.bbc.com/news/business-61298791` accessed 2022-05-15.

[51] Julien Armijo and Cédric Philibert. Flexible production of green hydrogen and ammonia from variable solar and wind energy. case study of chile and argentina. *International Journal of Hydrogen Energy*, 45, 05 2019.

[52] F. Kaspar, M. Borsche, U. Pfeifroth, J. Trentmann, J. Drücke, and P. Becker. A climatological assessment of balancing effects and shortfall risks of photovoltaics and wind energy in germany and europe. *Advances in Science and Research*, 16:119–128, 07 2019.

[53] International Renewable Energy Agency. *Geopolitics of the energy transformation: the hydrogen factor.* OCLC: 1301916739.

[54] European Commission. Directorate General for Energy., Enerdata., Cambridge Econometrics., Bölkow L. SystemTechnik (LBST)., and Trinomics B.V. *Study on energy prices, costs and subsidies and their impact on industry and households: final report.* Publications Office.

[55] T. Stützle and Holger H. Hoos. Max–min ant system. *Future Generation Computer Systems*, 16:889–914, 2000.

[56] C. García-Martínez, O. Cordón, and F. Herrera. A taxonomy and an empirical analysis of multiple objective ant colony optimization algorithms for the bi-criteria TSP. 180(1):116–148.

[57] M. Laumanns, L. Thiele, and E. Zitzler. An efficient, adaptive parameter variation scheme for metaheuristics based on the epsilon-constraint method. 169(3):932–942.

[58] S. Huband, P. Hingston, L. Barone, and L. While. A review of multiobjective test problems and a scalable test problem toolkit. 10(5):477–506.

[59] K. Socha and M. Dorigo. Ant colony optimization for continuous domains. 185(3):1155–1173.

[60] Hydrogen Council. Hydrogen scaling up : A sustainable pathway for the global energy transition, November 2017.

[61] Wikipedia. Box plot. `https://en.wikipedia.org/wiki/Box_plot` accessed 2022-05-20.

UNIVERSITÉ CATHOLIQUE DE LOUVAIN
École polytechnique de Louvain
Rue Archimède, 1 bte L6.11.01, 1348 Louvain-la-Neuve, Belgique | **www.uclouvain.be/epl**